

Transport coefficients of leptons in superconducting neutron star cores

P. S. Shternin*

Ioffe Institute, 26 Politekhnikeskaya st., St. Petersburg, 194021, Russia

(Dated: September 14, 2018)

I consider the thermal conductivity and shear viscosity of leptons (electrons and muons) in the nucleon neutron star cores where protons are in the superconducting state. I restrict the consideration to the case of not too high temperatures $T \lesssim 0.35T_{cp}$, where T_{cp} is the critical temperature of the proton pairing. In this case, lepton collisions with protons can be neglected. Charged lepton collision frequencies are mainly determined by the transverse plasmon exchange and are mediated by the character of the transverse plasma screening. In our previous works [Shternin & Yakovlev, Phys. Rev. D **75** 103004 (2007); **78** 063006 (2008)] the superconducting proton contribution to the transverse screening was considered in the Pippard limit $\Delta \ll \hbar q v_{Fp}$, where Δ is the proton pairing gap, v_{Fp} is the proton Fermi velocity, and $\hbar q$ is the typical transferred momentum in collisions. However, for large critical temperatures (large Δ) and relatively small densities (small q) the Pippard limit may become invalid. In the present study I show that this is indeed the case and that the older calculations severely underestimated the screening in a certain range of the parameters appropriate to the neutron star cores. As a consequence, the kinetic coefficients at $T \ll T_{cp}$ are found to be smaller than in previous calculations.

PACS numbers: 97.60.Jd, 52.25.Fi, 52.27.Ny, 26.60.Dd, 74.25.F-

I. INTRODUCTION

Neutron stars (NSs) are the most compact stars known in the Universe comprising about 1.5 solar masses in a ~ 12 km radius sphere. In their interiors, NSs contain superdense matter of largely unknown composition [1]. Their astrophysical manifestations are numerous, delivering signals in all bands of the electromagnetic spectra [2]. Moreover, gravitational waves from a binary NS merger were detected recently [3]. Understanding NSs requires modelling of various processes in their interiors. Important ingredients for this modelling are the transport coefficients of the superdense matter [4, 5].

In the present paper I discuss the thermal conductivity κ and shear viscosity η in NS cores of the simplest composition containing mainly neutrons (n) with admixture of protons (p), electrons (e), and muons (μ). Electrons and muons form relativistic degenerate almost ideal Fermi gases, while baryons (neutrons and protons) form non-ideal strongly-interacting Fermi liquid [1]. Transport coefficients are governed by the particle collisions. Leptons collide with themselves and with charged protons due to electromagnetic interaction, while collisions between baryons are mediated mainly by the strong interaction. To a good approximation, it is possible to consider lepton and baryon subsystems separately [6]. For instance for the thermal conductivity one writes $\kappa = \kappa_{e\mu} + \kappa_{np}$. In this case, when the lepton part, $\kappa_{e\mu}$ (or $\eta_{e\mu}$), is calculated, protons (or other charged baryons if present) are treated as passive scatterers.

Currently adopted calculations of the lepton contribution to transport coefficients of non-superfluid NS core matter were performed in Refs. [7–9] with a proper ac-

count for the screening of electromagnetic interaction following original ideas of Heiselberg et al. [10] and Heiselberg and Pethick [11]. Calculations of the nucleon part, κ_{np} and η_{np} , are more uncertain since one needs to rely on a certain many-body theory of nuclear matter. Transport coefficients in the nucleon sector are studied, for instance, in Refs. [12–15] and more complete list of references can be found in the recent review [4].

Nuclear matter in NS cores can be in the superfluid (paired) state due to an attractive component of the nuclear interaction [16–19]. Critical temperatures of the proton pairing $T_{cp}(n_B)$ and neutron pairing $T_{cn}(n_B)$ depend on the baryon number density n_B . Neutrons are believed to be paired in the singlet 1S_0 state at low densities (low Fermi momenta). In most models this type of the neutron pairing realizes in the NS inner crust, where the gas of free unbound neutrons coexists with the Coulomb lattice of ions and the degenerate electron gas. The singlet neutron pairing ceases in the core, where the 1S_0 channel of the nuclear interaction becomes repulsive. Instead, the neutron-neutron interaction becomes attractive in the triplet 3P_2 channel leading to the anisotropic paired state in the NS core. Proton number density is ~ 10 times smaller than the neutron one, therefore protons in the outer core are thought to be paired in the 1S_0 channel. In the inner core, where the proton number density increases, the 1S_0 proton pairing is thought to disappear. Calculations of critical temperature profiles for triplet neutron and singlet proton pairings in the NS core are very model-dependent [16, 17, 20]. Generally, the profiles $T_{cp}(n_B)$ and $T_{cn}(n_B)$ are bell-like, reaching maximum at some density within the core. The maximal critical temperature for protons is thought to be in the range $10^9 - 10^{10}$ K, while for triplet neutron superfluidity the corresponding values are found to be generally smaller, in the range of $10^8 - 5 \times 10^9$ K. For typi-

* pshternin@gmail.com

cal temperatures in the interiors of not too young NSs, $T \sim 10^8$ K [21], protons in a large part of the core are expected to be in the paired and hence superconducting state.

Neutron superfluidity does not produce immediate effect on the lepton contribution to the transport coefficients. In contrast, the superfluidity of protons affects $\kappa_{e\mu}$ and $\eta_{e\mu}$ in two aspects. The first one is the damping of the lepton-proton collisions due to the reduction of the number of the proton excitations. The lepton-proton scattering is damped roughly by the exponential factor $\exp(-\Delta/T)$, where Δ is the gap in the proton energy spectrum.¹ The second effect comes from the modification of the screening of the electromagnetic interactions which affects collisions between all charged particles including unpaired ones (leptons in the present case). Both these effects were investigated in Refs. [7, 8]. In these papers, the proton contribution to screening was taken in the so-called Pippard limit, $qv_{Fp} \gg \Delta$, where v_{Fp} is the proton Fermi velocity and q is the momentum transfer in collisions, both of which increase with density. In the present paper I show that this limit is inapplicable for the wide range of conditions relevant for NS cores, i.e. for not too high densities (small qv_{Fp}) or for relatively high gap values (high T_{cp}). The opposite, London limit, $\Delta \gg qv_{Fp}$ can be equally relevant for lepton scattering, and the transition between two limiting cases occurs roughly at the transition between the superconductors of the first and second kind.

The paper is organized as follows. In Sec. II the general formalism needed to calculate transport coefficients of npe μ matter of NS cores is briefly outlined and the results of Refs. [7, 8] for a normal (non-superfluid) case are reviewed. In Sec. III A the plasma screening properties in presence of the proton pairing are discussed and in Sec. III B–III D transport coefficients in this case are calculated. The results are summarized and discussed in Sec. IV. I conclude in Sec. V.

The consideration in this study is limited to small temperatures, $T \lesssim 0.35T_{cp}$ and the effects of magnetic fields are not included.

II. GENERAL EXPRESSIONS

Transport coefficients in NS cores can be calculated in the framework of the transport theory of Fermi liquids [22] adapted for multicomponent systems [4, 6, 23]. Below I closely follow Refs. [7, 8] and omit the details.

Thermal conductivity κ_c and shear viscosity η_c of particle species c can be conveniently written as

$$\kappa_c = \frac{\pi^2 T n_c}{3m_c^*} \tau_c^\kappa, \quad \eta_c = \frac{p_{Fc}^2 n_c}{5m_c^*} \tau_c^\eta, \quad (1)$$

where n_c is the number density of the corresponding species, p_{Fc} is their Fermi momentum, and m_c^* is their effective mass on the Fermi surface. The quantities $\tau_c^{\kappa,\eta}$ are effective relaxation times which are generally not the same for different transport problems (thermal conductivity and shear viscosity in present case, as indicated by the corresponding superscripts here and in the rest of the paper) and need to be determined from the transport theory.

The effective relaxation times $\tau_c^{\kappa,\eta}$ are found from the solution of a system of coupled transport equations. However, for strongly degenerate matter in NS cores it is enough to rely on the simplest variational solution of this system [4, 7, 8] (see, however, Sec. III D). Then the problem of finding effective relaxation times reduces to a system of algebraic equation

$$1 = \sum_i (\nu_{ci} \tau_c + \nu'_{ci} \tau_i), \quad (2)$$

where indices c, i number particles species and the effective collision frequencies ν_{ci} and ν'_{ci} are related to the transport cross-sections as shown below. The correction to the variational solution for lepton transport coefficients in normal matter was found to be within 10% [7, 8] which is unimportant for practical applications. The frequencies ν_{ci} describe relaxation due to collisions of particle species c with all other particles including the passive scatterers. The primed quantities ν'_{ci} are the mixing terms. Notice, that the summation in Eq. (2) is carried over all particle species in both terms, so that the actual collision frequency for collisions of like particles is $\nu_{cc} + \nu'_{cc}$. These two parts are kept separated for convenience.

Collision frequencies are calculated by integrating the squared matrix element $|M_{ci}|^2$ of corresponding interaction over the available phase space with certain phase factors. Consider particle collisions $c, i \rightarrow c', i'$. Primes here mark the particle states after the collision. Due to a strong degeneracy, the particle states before and after the collision can be placed on the respective Fermi surfaces whenever possible, hence the absolute values of input and output momenta are fixed: $p_c = p_{c'} = p_{Fc}$ and $p_i = p_{i'} = p_{Fi}$. Owing to the momentum conservation, the relative orientation of the four participating momenta is fixed by two angular variables. In case of electromagnetic collisions, the convenient pair of variables is the absolute value of the transferred momentum q , where $\mathbf{q} = \mathbf{p}_{c'} - \mathbf{p}_c$, and the angle ϕ between the vectors $\mathbf{p}_c + \mathbf{p}_{c'}$ and $\mathbf{p}_i + \mathbf{p}_{i'}$. Notice, that these two vectors are transverse to \mathbf{q} . It is instructive to introduce the spin-averaged squared matrix element $\mathcal{Q}_{ci}(\omega, q, \phi) = (1 + \delta_{ci})^{-1} \sum_{\text{spins}} |M_{ci}|^2 / 4$, where the factor $(1 + \delta_{ci})^{-1}$ is included in order to avoid double counting of the same collisions when antisymmetrized amplitudes are used. In general, \mathcal{Q}_{ci} depends also on the transferred energy $\omega = \epsilon_{c'} - \epsilon_c$, where ϵ_c is the particle energy. In degenerate matter, ω is of the order of T and therefore small. In the limit $\omega \ll qv_{Fi}$, the collision frequencies to

¹ Throughout the paper the natural unit system is used, where $\hbar = c = k_B = 1$.

be used in (2) are [7, 8]

$$\nu_{ci}^\kappa = \frac{3T^2 m_c^* m_i^{*2}}{4\pi^4 p_{Fc}} \times \left\langle \frac{\omega^2}{\pi^2 T^2} \left(1 + \left[\frac{\pi^2 T^2}{3\omega^2} - \frac{1}{6} \right] \frac{q^2}{p_{Fi}^2} \right) \mathcal{Q}_{ci} \right\rangle, \quad (3)$$

$$\nu'_{ci}{}^\kappa = -\frac{3T^2 p_{Fi} m_c^* m_i^*}{4\pi^4 p_{Fc}^2} \times \left\langle \frac{\omega^2}{\pi^2 T^2} \sqrt{\left(1 - \frac{q^2}{4p_{Fc}^2} \right) \left(1 - \frac{q^2}{4p_{Fi}^2} \right)} \cos \phi \mathcal{Q}_{ci} \right\rangle, \quad (4)$$

$$\nu_{ci}^\eta = \frac{3T^2 m_c^* m_i^{*2}}{4\pi^4 p_{Fc}} \left\langle \frac{q^2}{p_{Fc}^2} \left(1 - \frac{q^2}{4p_{Fc}^2} \right) \mathcal{Q}_{ci} \right\rangle, \quad (5)$$

$$\nu'_{ci}{}^\eta = -\frac{3T^2 p_{Fi} m_c^* m_i^*}{4\pi^4 p_{Fc}^2} \times \left\langle \frac{q^2}{p_{Fc}^2} \sqrt{\left(1 - \frac{q^2}{4p_{Fc}^2} \right) \left(1 - \frac{q^2}{4p_{Fi}^2} \right)} \cos \phi \mathcal{Q}_{ci} \right\rangle, \quad (6)$$

where the angular brackets denote phase-space integration

$$\langle \cdot \rangle = \int_0^\infty dw \frac{(w/2)^2}{\sinh^2(w/2)} \int_0^{q_m} dq \int_0^\pi d\phi \cdot, \quad (7)$$

$$\mathcal{Q}_{ci} = 16\pi^2 \alpha_f^2 Z_c^2 Z_i^2 \left(\frac{L_l}{|q^2 + \Pi_l(\omega, q)|^2} - 2\text{Re} \frac{v_{Fc} v_{Fi} L_{tl}}{(q^2 + \Pi_l(\omega, q))(q^2 + \Pi_t(\omega, q))^*} + \frac{v_{Fc}^2 v_{Fi}^2 L_t}{|q^2 + \Pi_t(\omega, q)|^2} \right), \quad (9)$$

where the numerators are

$$L_l = \left(1 - \frac{q^2}{4m_c^{*2}} \right) \left(1 - \frac{q^2}{4m_i^{*2}} \right), \quad (10)$$

$$L_{tl} = \sqrt{\left(1 - \frac{q^2}{4p_{Fc}^2} \right) \left(1 - \frac{q^2}{4p_{Fi}^2} \right)} \cos \phi, \quad (11)$$

$$L_t = \left(1 - \frac{q^2}{4p_{Fc}^2} \right) \left(1 - \frac{q^2}{4p_{Fi}^2} \right) \cos^2 \phi + \frac{q^2}{4p_{Fc}^2} + \frac{q^2}{4p_{Fi}^2}. \quad (12)$$

In case of identical particles, \mathcal{Q}_{cc} also contains an exchange contribution from the interference between two scattering channels with the final states interchanged. However, for the electromagnetic collisions, small momentum transfer $q \ll p_{Fc}$ dominates the scattering, interference corrections are of the next order in q and are found to be negligible [7, 8].

As follows from Eq. (9), \mathcal{Q}_{ci} has contributions from longitudinal, transverse, and mixed parts of electromag-

$w = \omega/T$, and $q_m = \min(2p_{Fc}, 2p_{Fi})$. Dependence of \mathcal{Q}_{ci} on ω determines the temperature behavior of collision frequencies and hence of the corresponding transport coefficients. In traditional transport theory of Fermi systems, the transition probability is assumed to be independent of ω . Then each collision frequency in Eqs. (3)–(6) obeys $\nu_{ci} \propto T^2$ scaling which according to Eqs. (1)–(2) results in standard dependencies $\kappa \propto T^{-1}$ and $\eta \propto T^{-2}$. These relations hold, for instance, for the transport coefficients in the nucleon sector, e.g. [4].

Consider leptonic (electrons and muons) subsystem. Leptons collide with all charged particles due to electromagnetic interaction. The matrix element of this interaction can be written as a sum of the longitudinal and transverse parts

$$M_{ci} = 4\pi\alpha_f \left(\frac{J_c^{(0)} J_i^{(0)}}{q^2 + \Pi_l(\omega, q)} - \frac{\mathbf{J}_{c,t} \cdot \mathbf{J}_{i,t}}{q^2 - \omega^2 + \Pi_t(\omega, q)} \right), \quad (8)$$

where $\alpha_f \approx 1/137$ is the fine structure constant, $J_c^{(0)}$ and $\mathbf{J}_{c,t}$ are time-like and transverse (with respect to \mathbf{q}) space-like components of the transition current, respectively, and Π_l and Π_t are the longitudinal and transverse polarization functions, respectively.

The transition four-current in Eq. (8) is $J_c^\lambda = Z_c \bar{u}(\mathbf{p}_{c'}) \gamma^\lambda u(\mathbf{p}_c) / (2\sqrt{\epsilon_c \epsilon_{c'}})$, where Z_c is the charge number of the particle species c , γ^λ is a Dirac matrix, and $u(\mathbf{p}_c)$ is the Dirac spinor. Performing spin summations (in the limit $\omega \ll qv_{Fi}$), one obtains [7, 8, 24]

netic interaction. Moreover, due to a specific $\cos \phi$ dependence in Eqs. (3)–(6) and (10)–(11), the mixed term does not contribute to ‘direct’ collision frequencies (3) and (5), so one can write $\nu_{ci} = \nu_{ci}^l + \nu_{ci}^t$. In contrast, only the mixed term contributes to the primed collision frequencies, $\nu'_{ci} = \nu_{ci}^{tl}$ [7, 8]. In the non-relativistic limit $v_{Fc/i} \ll 1$ and the transverse part of the interaction is unimportant. However, it turns out that for relativistic particles this part gives the dominant contribution because of the weaker screening. The leading q^{-4} dependence of \mathcal{Q}_{ci} is regularized at small q by the polarization functions Π_l and Π_t which play the central role in determining the collision frequencies. Characters of the longitudinal and transverse screening are very different. It is enough to consider screening in the limits of small $q \ll p_{Fi}$ and $\omega \ll \mu_i$, where μ_i is the chemical potential of the i species, and also in the static limit $\omega \ll qv_{Fi}$. Then the longitudinal part of the interaction is screened

on a static Thomas-Fermi scale

$$\Pi_l(\omega, q) = q_{\text{TF}}^2 \equiv \frac{4\alpha_f}{\pi} \sum_i Z_i^2 m_i^* p_{\text{Fi}}, \quad (13)$$

where q_{TF} is the Thomas-Fermi screening momentum. In contrast, the transverse screening is dynamical

$$\Pi_t(\omega, q) = i \frac{\pi \omega}{4} q_t^2 \equiv i \frac{\omega}{q} \alpha_f \sum_i Z_i^2 p_{\text{Fi}}^2, \quad (14)$$

where q_t is a characteristic transverse momentum. Therefore the screening scale of the transverse part of the interaction is $\sim (\omega q_t^2)^{1/3} \ll q_{\text{TF}}$ [examine the denominator in the third term in Eq. (9)]. This leads to dominant contribution of the transverse interaction to the collision frequencies, $\nu_{ci}^t \gg \nu_{ci}^l, \nu_{ci}^{tl}$. As a consequence, the system (2) decouples, and in the leading order $\tau_c = (\sum_i \nu_{ci}^t)^{-1}$. Retaining only the transverse contribution and the leading order in q in Eqs. (3)–(6), one gets the following expressions for the lepton thermal conductivity and shear viscosity in normal matter [4, 7, 8]

$$\kappa_{e\mu} = \frac{\pi^2}{54\zeta(3)} \frac{p_{\text{Fe}}^2 + p_{\text{F}\mu}^2}{\alpha_f}, \quad (15)$$

$$\eta_{e\mu} = \frac{1.1}{\alpha_f} \frac{n_e^2 + n_\mu^2}{q_t^{1/3}} T^{-5/3}, \quad (16)$$

where $\zeta(3)$ is the Riemann zeta-function. Notice the unusual temperature behavior of $\kappa_{e\mu}$ and $\eta_{e\mu}$ in comparison to the standard Fermi-liquid results. This is a consequence of the dynamical character of the transverse screening. The different powers of T in Eqs. (15) and (16) are traced back to the different leading orders in q for the thermal conductivity (q^0) and shear viscosity (q^2) problems in Eqs. (3)–(6). Expression (15) is a good approximation to the exact result, which includes all contributions to collision frequencies. For the shear viscosity, the dominance of the transverse part of interaction is not so strong, and Eq. (16) can actually result in a strong overestimation of the shear viscosity coefficient [8, 13]. In this case all terms need to be retained.

III. LEPTON TRANSPORT COEFFICIENTS IN SUPERCONDUCTING NS CORES

Shternin and Yakovlev [7, 8] also calculated $\kappa_{e\mu}$ and $\eta_{e\mu}$ in the case when the protons are in the paired state. They noticed that the proton pairing changes the character of transverse plasma screening from the dynamical to the static one restoring the Fermi-liquid behavior of transport coefficients. Below I show that this qualitative result is correct, but the treatment of screening in Refs. [7, 8] was incomplete. For simplicity, I restrict myself to the case of well-developed superconductivity $T \lesssim 0.2\Delta$. For 1S_0 pairing, dependence of the superfluid gap on temperature can be approximated as [25]

$$\frac{\Delta}{T} = \sqrt{1-t} \left(1.456 - \frac{0.157}{\sqrt{t}} + \frac{1.764}{t} \right), \quad (17)$$

where $t = T/T_{cp}$. Thus the condition $T \lesssim 0.2\Delta$ translates to $T/T_{cp} \lesssim 0.35$. In this case, first of all, lepton-proton collisions can be neglected, and, second, the zero-temperature limit for the proton polarization function can be used. Provided high expected values of T_{cp} , this limit is comfortably satisfied at $T \lesssim 10^8$ K.

A. Plasma screening in presence of proton pairing

Pairing of protons, which are charged particles, modifies the screening of the electromagnetic interaction. Up to the order Δ/μ_p , the static longitudinal screening does not change [26, 27] and Π_l is given by Eq. (13). In contrast, the transverse screening modifies. At low T , the dominant contribution to screening comes from protons. In the zero-temperature limit $T \rightarrow 0$ in the Bardeen-Cooper-Schrieffer (BCS) theory the static ($\omega \rightarrow 0$) transverse polarization function can be written as [28]

$$\Pi_t(0, q) = q_M^2 J(\zeta), \quad (18)$$

where $\zeta = qv_{\text{F}p}/\Delta = \pi q\xi$, ξ is the coherence length, and q_M is the Meissner screening momentum (Meissner mass)

$$q_M^2 = \frac{4\alpha_f}{3\pi} p_{\text{F}p}^2 v_{\text{F}p}. \quad (19)$$

The function $J(\zeta)$ in Eq. (18) is [28]

$$\begin{aligned} J(\zeta) &= \frac{3}{8} \int_{-\infty}^{\infty} d\eta \int_{-1}^1 \frac{dx (1-x^2)}{\sqrt{\eta^2+1} (\eta^2+1 + (\zeta x)^2/4)} \\ &= \frac{3}{4} \int_{-1}^1 dx (1-x^2) \frac{2\text{ArcSinh}(\zeta x/2)}{\zeta x \sqrt{1 + (\zeta x)^2/4}}. \end{aligned} \quad (20)$$

In principle, the integration over x in the second line in Eq. (20) can be performed analytically with the result being expressed via the polylogarithmic functions.

The function $J(\zeta)$ is plotted in Fig. 1. At small ζ (small momentum $q \ll \xi^{-1}$), which corresponds to the London limit, $J(\zeta) = 1$. In this limit, the transverse screening is independent of Δ and the screening momentum is equal to q_M . The real transverse photons obey the Meissner mass q_M in this limit. This leads to the Meissner effect in superconductors. In the opposite, Pippard limit, $\zeta \gg 1$ and Π_t is inversely proportional to ζ as shown by the dashed line in Fig. 1. The asymptotic expression in the Pippard limit reads $J(\zeta) = 3\pi^2/(4\zeta)$. In this limit, the characteristic transverse screening momentum is $q_P = (3\pi^2\Delta q_M^2/(4v_{\text{F}p}))^{1/3}$. This expression resembles the screening momentum in the non-superfluid case, with Δ in place of ω and q_M in place of q_t . In the Pippard limit, contrary to the London limit, the screening depends on Δ .

In Fig. 2, the characteristic transverse screening momenta q_M (dashed lines) and q_P (dash-dotted lines for $T_{cp} = 10^9$ K and double-dot-dashed lines for $T_{cp} =$

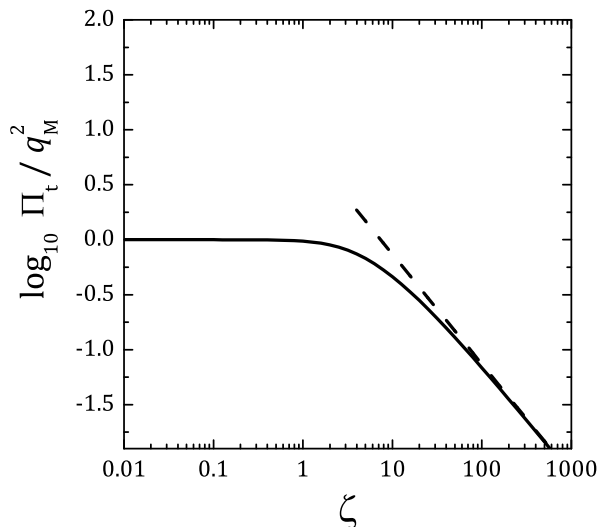


Figure 1. Proton contribution to the zero-temperature transverse polarization function in the static limit. Polarization function is normalized to q_M^2 . Dashed line shows the asymptote in the Pippard limit.

10^{10} K) are compared with the longitudinal screening momentum q_{TF} (solid lines). The momenta in the plot are normalized to $2p_{\text{Fe}}$, which is the maximum momentum transfer in electron-electron collisions. Thick and thin lines correspond to two widely used equations of state (EOSs) of dense nucleon matter in NS cores. Namely, by the abbreviation HHJ (thick lines) I denote the EOS constructed by Heiselberg and Hjorth-Jensen [29] as an analytical parameterization of the variational EOS by Akmal et al. [30]. Specifically, I use the model with the parameter $\gamma = 0.6$ of Ref. [29]; this model was designated as APR I in Ref. [31] and the NS properties with such EOS can be found there. With thin lines I show the results for one of the EOSs based on the Brussels-Skyrme nucleon interaction functionals, namely the BSk21 model [32]. Both EOSs satisfy the equilibrium conditions with respect to the weak processes. Unless otherwise indicated, the proton effective mass is set to $m_p^* = 0.8m_u$, where m_u is the nucleon mass unit. Two EOSs are different in the particle fractions, however the results shown in Fig. 2 are qualitatively same. As in the normal matter, characteristic transverse screening momenta (q_M or q_P) are much smaller than the longitudinal one. As a consequence, the transverse part of the interaction dominates in the presence of proton superconductivity as well.

In Refs. [7, 8] it was assumed that the typical transferred momentum q is not so small, so that the Pippard limit gives appropriate description of the transverse plasma screening in NS cores. In fact, which limit, London or Pippard, gives the dominant contribution depends on the value of ζ at $q = q_M$. This point was overlooked in Refs. [7, 8]. It is hence convenient to introduce the parameter $A \equiv \zeta(q = q_M) = v_{\text{Fp}} q_M / \Delta$. In the BCS approximation, this parameter is related to the fa-

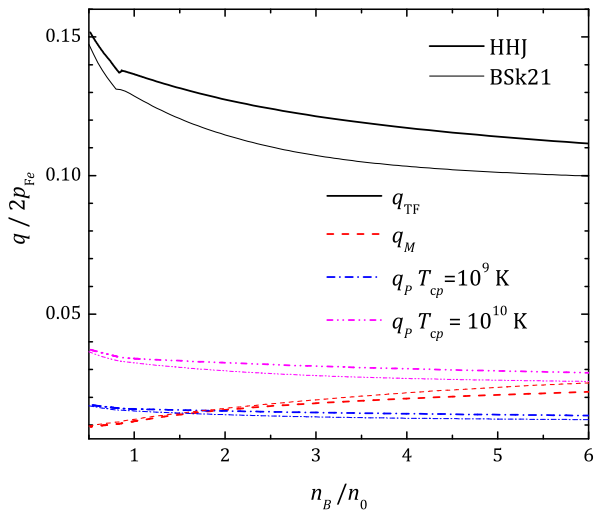


Figure 2. (Color online). Ratios of characteristic screening momenta to $2p_{\text{Fe}}$ versus baryon density (in units of the nuclear saturation density $n_0 = 0.16 \text{ fm}^{-3}$) for two EOSs described in the text. Thick lines correspond to the HHJ EOS, while thin lines show the results for the BSk21 EOS. Solid lines show the longitudinal (Thomas-Fermi) screening momentum q_{TF} , dashed lines give the Meissner momentum q_M . Dash-dotted and double-dot-dashed lines show the characteristic screening momenta in Pippard limit for $T_{\text{cp}} = 10^9$ K and 10^{10} K, respectively.

miliar Ginzburg-Landau coherence parameter \varkappa , namely $\varkappa = \lambda_L / \xi = \pi / A$, where $\lambda_L = q_M^{-1}$ is the London penetration depth. The value of \varkappa determines the superconductivity type. The transition from type I superconductor to type II superconductor occurs at $\varkappa > 1/\sqrt{2}$ as type-I [28, 33], which corresponds to $A < \sqrt{2}\pi \approx 4.4$.² The parameter A can be written as

$$A = 1.12 \left(\frac{x_p}{0.1} \right)^{5/6} \left(\frac{n_B}{n_0} \right)^{5/6} \left(\frac{m_p^*}{m_u} \right)^{-3/2} \frac{0.5 \text{ MeV}}{\Delta}, \quad (21)$$

where $n_0 = 0.16 \text{ fm}^{-3}$ is the nuclear saturation density. In Fig. 3, the parameter A is plotted for two EOSs discussed above and for $\Delta = 1 \text{ MeV}$. This corresponds to $T_{\text{cp}} \approx 6.5 \times 10^9 \text{ K}$ [see Eq. (17) at $T = 0$]. For this large Δ , most of the core forms type-II superconductor [35]. Since A is inversely proportional to Δ , it is higher for lower Δ (lower T_{cp}). For the NS core conditions, A can

² Notice, that this criterion modifies in the superfluid-superconducting mixtures [34] which is quite possible in NS cores where (in large part at least) neutrons can also be in the superfluid state. According to Ref. [34], the point $\varkappa = 1/\sqrt{2}$ does not separate the topologically different type-I and type-II phases in this case, and situation is more complicated. Since the results of the present paper are not affected by these complications, we will nevertheless call the region where $\varkappa \geq 1/\sqrt{2}$ as type-II superconductivity region, and where $\varkappa < 1/\sqrt{2}$ as type-I superconductivity region for simplicity.

vary in the range $0.1 \div 100$. Figure 1 shows that these values correspond to the intermediate region between the London and Pippard limits, thus one can expect that neither of these limits is strictly applicable in NS cores, and the general form of Π_t should be used for calculating the transport coefficients. This is demonstrated in the next Section.

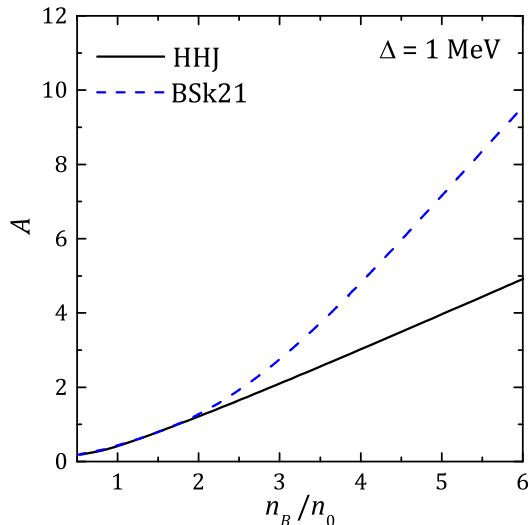


Figure 3. (Color online). The coherence scale parameter A as a function of the total baryon density for two selected EOSs. Effective masses are set to $m_p^* = 0.8m_u$ and $\Delta = 1$ MeV.

B. Calculation of transport coefficients in the leading order

According to the discussion in Secs. II and III A (see also Fig. 2), the dominant contribution to the lepton collision frequencies comes from the transverse part of the electromagnetic interaction. In addition, since the screening is weak, the lowest order in q in Eqs. (3)–(6), (9)–(12) gives the leading contribution to transport coefficients. In order to calculate the transverse collision frequencies ν_{ci}^t , the integrals

$$I_n^t(A, q_M) = \int_0^{q_m} \frac{dq q^n}{(q^2 + q_M^2 J(\zeta))^2} \quad (22)$$

are needed. The exponent $n = 0$ in Eq. (22) gives the leading order contribution to the thermal conductivity problem, while for the shear viscosity the leading order is given by $n = 2$ (Sec. II). Retaining only the leading contributions one gets the following results for the lepton thermal conductivity and shear viscosity

$$\kappa_{e\mu}^{t, \text{Lead}} = \frac{5}{72\pi\alpha_f^2 T} [I_0^t(A, q_M)]^{-1}, \quad (23)$$

$$\eta_{e\mu}^{t, \text{Lead}} = \frac{3\pi}{10\alpha_f^2 T^2} \frac{n_e^2 + n_\mu^2}{p_{Fe}^2 + p_{F\mu}^2} [I_2^t(A, q_M)]^{-1}. \quad (24)$$

Let us analyze an asymptotic behavior of the integrals (22). In the weak-screening limit $q_M \ll q_m$ it is enough to extend the upper integration limit to infinity. Then, the low- A asymptote becomes

$$I_n^t = \frac{\pi}{4q_M^{3-n}}, \quad A \ll 1, \quad (25)$$

while the high- A asymptotes are

$$I_0^t = \frac{4A}{9\pi^2 q_M^3}, \quad I_2^t = \frac{4A^{1/3}}{9q_M} \frac{2^{2/3}\pi^{1/3}}{3^{5/6}}, \quad A \gg 1. \quad (26)$$

Remarkably, the low- A asymptote (25), which corresponds to the London limit, is independent of A and hence of Δ . This is a consequence of the independence of the Meissner momentum q_M of the gap value. The case of large A , Eq. (26), corresponds to the Pippard limit that was employed in Refs. [7, 8]. In the intermediate case, the integrals I_0^t and I_2^t were fitted by the analytic expressions to facilitate their use in applications. These expressions are given in the Appendix. Substituting the limiting expressions (25)–(26) into Eqs. (23)–(24), one obtains the asymptotic expressions for the thermal conductivity and shear viscosity

$$\kappa_{e\mu}^{\text{Lon}} = \frac{5q_M^3}{18\pi^2\alpha_f^2 T}, \quad (27)$$

$$\eta_{e\mu}^{\text{Lon}} = \frac{6q_M}{5\alpha_f^2 T^2} \frac{n_e^2 + n_\mu^2}{p_{Fe}^2 + p_{F\mu}^2}, \quad (28)$$

$$\kappa_{e\mu}^{\text{Pip}} = \frac{5p_{Fp}^2 \Delta}{24\alpha_f T}, \quad (29)$$

$$\eta_{e\mu}^{\text{Pip}} = \frac{1.71 p_{Fp}}{\alpha_f^{5/3} T^2} \frac{n_e^2 + n_\mu^2}{p_{Fe}^2 + p_{F\mu}^2} \left(\frac{\Delta}{p_{Fp} c} \right)^{1/3}, \quad (30)$$

where the superscripts Lon and Pip correspond to the London and Pippard approximations to Π_t , respectively.

Comparing the expressions (25) and (26) one can roughly estimate that the crossover between the two limiting cases occurs at $A \approx 17.5$ for $n = 0$ and at $A \approx 6.8$ for $n = 2$. From Fig. 3, one concludes that for large $\Delta \sim 1$ MeV or for small n_B if Δ is lower, the Pippard limit used in Refs. [7, 8] is inapplicable. To illustrate the possible degree of inaccuracy of the older results, let us construct the ratio $R(A)$ of the leading contribution to transverse collision frequency to those calculated in the Pippard limit: $\nu_t^{\text{Lead}} = \nu_t^{\text{Pip}} R(A)$. This ratio is plotted as a function of A in Fig. 4 for $n = 0$ (thermal conductivity, solid lines) and $n = 2$ (shear viscosity, dashed lines). The plot clearly shows underestimation of the collision frequencies, and, hence overestimation of the transport coefficients by the Pippard limiting values (29)–(30). For small A and $n = 0$ this overestimation reaches two orders of magnitude. For the shear viscosity problem ($n = 2$), the overestimation is modest because of the weaker dependence of the collision frequencies on the screening momentum (Sec. II). Thin lines in Figure 4 show the same

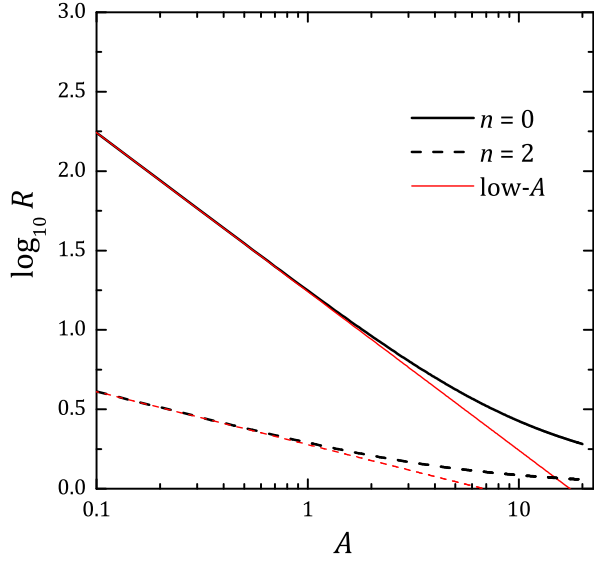


Figure 4. (Color online). The ratio $R(A)$ for $n = 0$ (solid lines) and $n = 2$ (dashed lines). Thin lines represent the low- A approximation (25).

factors, where the London asymptotic expression for collision frequencies is used in place of $\nu^{t, \text{Lead}}$. One concludes, that the London limit for screening is appropriate in the case of type-II superconductivity, but for large values of A it becomes inapplicable. Fig. 4 shows that both asymptotic limits generally underestimate the collision frequencies and overestimate the transport coefficients. This is because of an overestimation of the screening at large q by the London expression and at small q by the Pippard expression, see Fig. 1.

For illustration, the same ratios R are plotted in Fig. 5 now as functions of the baryon density for the HHJ EOS and three values of $T_{cp} = 10^{10}$ K (solid lines), 3×10^9 K (dashed lines), and 10^9 K (dash-dotted lines). Figure 5(a) shows the results appropriate for the thermal conductivity ($n = 0$), while for the shear viscosity problem ($n = 2$), R is shown in Fig. 5(b). Like in Fig. 4, thin lines give the ratio R calculated with London limiting expression. For the highest shown critical temperature, $T_{cp} = 10^{10}$ K, R is largest and the London expression is a good approximation for $n = 0$ in the whole shown range of densities and for $n_B \lesssim 3n_0$ for $n = 2$. With decreasing T_{cp} (increasing A), the ratio R lowers down and the applicability range of the London limiting expression shifts to lower densities. For instance, for $T_{cp} = 10^9$ K and $n = 2$ the London approximation is always inaccurate, as seen from a comparison of thin and thick dash-dotted lines in Fig. 5(b).

C. Kinematic corrections

In the previous section the leading order contribution to the collision frequencies was discussed. However, as

was mentioned at the end of the Sec. II, this approximation can be inaccurate, especially for the shear viscosity and in principle the full result that follows from Eqs. (2)–(6) and (9)–(12) shall be used [4, 8, 13]. The main corrections come from the inclusion of the longitudinal part of the interaction, and from the kinematic corrections of high- q powers in Eqs. (3)–(6) and (10)–(12). Going beyond the long-wavelength and static limit in polarization functions is not necessary, since the possible difference would be sizable at large q , where the q^2 term dominates in the denominators in Eq. (9). Since both longitudinal and transverse screening are static, the integration over w in Eqs. (3)–(6) can be performed analytically, as well as the integration over ϕ , leaving one with the following result for the thermal conductivity collision frequencies

$$\nu_{ci}^{\kappa} = \nu_{ci}^{\kappa, t} + \nu_{ci}^{\kappa, l}, \quad (31)$$

$$\begin{aligned} \nu_{ci}^{\kappa, t} &= \frac{8\pi\alpha_f^2 T^2 p_{Fc} p_{Fi}^2}{5m_c^*} \\ &\times \int_0^{q_m} dq \frac{\left(1 + \frac{q^2}{4p_{Fc}^2}\right)^2 \left(1 + \frac{q^2}{4p_{Fi}^2}\right)}{(q^2 + q_M^2 J(\zeta))^2}, \end{aligned} \quad (32)$$

$$\begin{aligned} \nu_{ci}^{\kappa, l} &= \frac{16\pi\alpha_f^2 T^2 m_c^* m_i^{*2}}{5p_{Fc}} \\ &\times \int_0^{q_m} dq \frac{\left(1 + \frac{q^2}{4p_{Fc}^2}\right) \left(1 - \frac{q^2}{4m_c^{*2}}\right) \left(1 - \frac{q^2}{4m_i^{*2}}\right)}{(q^2 + q_{TF}^2)^2}, \end{aligned} \quad (33)$$

$$\begin{aligned} \nu_{ci}^{\nu} &= \frac{16\pi\alpha_f^2 T^2 m_i^* p_{Fi}}{5} \\ &\times \int_0^{q_m} dq \frac{\left(1 - \frac{q^2}{4p_{Fc}^2}\right) \left(1 - \frac{q^2}{4p_{Fi}^2}\right)}{(q^2 + q_{TF}^2)(q^2 + q_M^2 J(\zeta))} \end{aligned} \quad (34)$$

and similarly for the shear viscosity collision frequencies

$$\nu_{ci}^{\eta} = \nu_{ci}^{\eta, t} + \nu_{ci}^{\eta, l}, \quad (35)$$

$$\begin{aligned} \nu_{ci}^{\eta, t} &= \frac{2\pi\alpha_f^2 T^2 p_{Fi}^2}{m_c^* p_{Fc}} \\ &\times \int_0^{q_m} dq q^2 \frac{\left(1 - \frac{q^4}{16p_{Fc}^4}\right) \left(1 + \frac{q^2}{4p_{Fi}^2}\right)}{(q^2 + q_M^2 J(\zeta))^2}, \end{aligned} \quad (36)$$

$$\begin{aligned} \nu_{ci}^{\eta, l} &= \frac{4\pi\alpha_f^2 T^2 m_c^* m_i^{*2}}{p_{Fc}^3} \\ &\times \int_0^{q_m} dq q^2 \frac{\left(1 - \frac{q^2}{4p_{Fi}^2}\right) \left(1 - \frac{q^2}{4m_c^{*2}}\right) \left(1 - \frac{q^2}{4m_i^{*2}}\right)}{(q^2 + q_{TF}^2)^2}, \end{aligned} \quad (37)$$

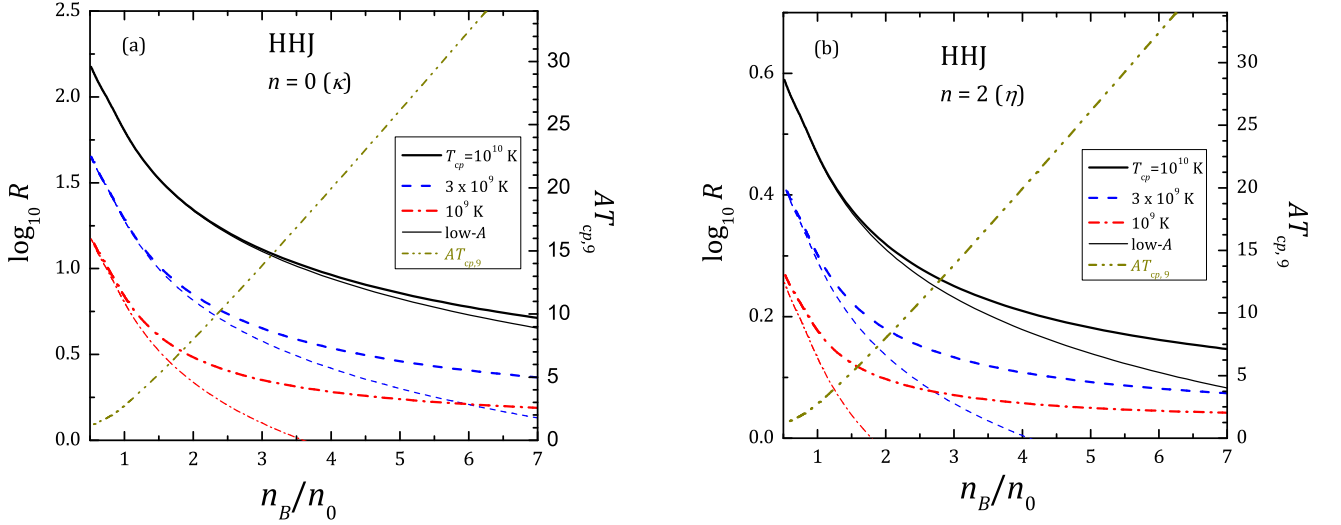


Figure 5. (Color online). The ratios R for (a) thermal conductivity ($n = 0$) and (b) shear viscosity ($n = 2$) as function of n_B for the HHJ equation of state and three values of $T_{cp} = 10^{10}$ K (solid lines), 3×10^9 K (dashed lines), and 10^9 K (dash-dotted lines). Thin lines give low- A approximation, where the interaction is screened by the pure Meissner mass. Double-dot-dashed lines show with right vertical scales the combination $AT_{cp,9}$ which is independent of T_{cp} . Here $T_{cp,9} \equiv T_{cp}/(10^9 \text{ K})$.

$$\nu_{ci}^{\eta} = \frac{4\pi\alpha_f^2 T^2 m_i^* p_{Fi}}{p_{Fc}^2} \times \int_0^{q_m} \frac{dq q^2 \left(1 - \frac{q^2}{4p_{Fc}^2}\right) \left(1 - \frac{q^2}{4p_{Fi}^2}\right)}{(q^2 + q_{TF}^2)(q^2 + q_M^2 J(\zeta))}. \quad (38)$$

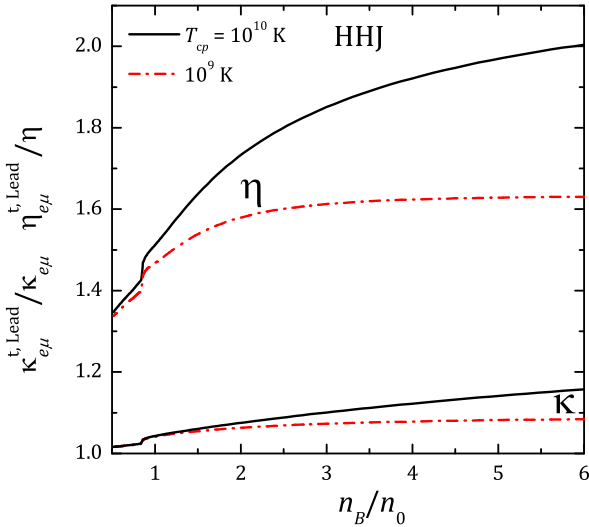


Figure 6. (Color online). Comparison of the thermal conductivity and shear viscosity in the leading approximation, Eqs. (23)–(24), to the results of complete calculations. Upper pair of curves shows the ratio $\eta_{e\mu}^{t, \text{Lead}}/\eta_{e\mu}$, while lower pair of curves marked κ shows $\kappa_{e\mu}^{t, \text{Lead}}/\kappa_{e\mu}$. Results for the HHJ EOS are shown and for two values of the proton critical temperature. $T_{cp} = 10^{10}$ K (solid lines) and 10^9 K (dashed lines). Variational solutions are employed. See text for details.

Thus in order to calculate the transverse part of the collision frequencies, $\nu_{ci}^{\kappa, t}$ and $\nu_{ci}^{\eta, t}$, including all kinematic corrections one needs integrals I_n^t defined in Eq. (22) up to $n = 8$. Similarly, to calculate longitudinal contributions, $\nu_{ci}^{\kappa, l}$ and $\nu_{ci}^{\eta, l}$, analogous longitudinal integrals

$$I_n^l(q_{TF}) = \int_0^{q_m} \frac{dq q^n}{(q^2 + q_{TF}^2)^2} \quad (39)$$

are required. These are standard integrals, and their explicit expressions up to $n = 8$ can be found, for instance, in the Appendix in Ref. [8]. Finally, to calculate the mixing terms, we need integrals

$$I_n^{tl}(A, q_M, q_{TF}) = \int_0^{q_m} \frac{dq q^n}{(q^2 + q_{TF}^2)(q^2 + q_M^2 J(\zeta))} \quad (40)$$

up to $n = 6$.

In Fig. 6, the results of full calculations which are based on Eqs. (31)–(38) and Eq. (2) are compared with the leading-order results (23)–(24) for two values of the critical temperature, $T_{cp} = 10^9$ K and 10^{10} K. Clearly, the kinematic corrections to the thermal conductivity coefficient can be safely ignored in applications. However, the leading-order expression (24) overestimates the shear viscosity by 50% for $T_{cp} = 10^9$ and up to a factor of two for $T_{cp} = 10^{10}$ K, since in the latter case the transverse screening momentum is larger, see Fig. 2. It is thus advisable to go beyond the leading-order expression when calculating $\eta_{e\mu}$. A detailed analysis of various corrections shows that it is necessary to include all three contributions – transverse, longitudinal, and mixed – but it is enough to use the lowest-order terms in q , namely retain only q^2 in numerators for each of these terms. In this approximation, $\eta_{e\mu}$ stays within 10% of the total result. The lowest-order contribution to $\nu_{ci}^{\eta, t}$ is discussed in the

previous section, while the explicit leading-order expression for $\nu_{ci}^{\eta,l}$ is given in the Appendix, Eq. (A.6). It remains to consider the leading-order contribution to ν_{ci}^{η} . Because of q^2 in the numerator and since $q_M \ll q_{TF}$, it is possible to neglect the transverse screening in Eq. (38) [8]. Then the integration over q is trivial. Explicit result is given in Eq. (A.7). Notice, that this procedure does not work for ν_{ci}^{κ} , Eq. (34). However, as discussed before, ν_{ci}^{κ} is actually not needed.

D. Corrections to variational solution

Up to now the simplest variational solution of the system of transport equations was employed. However, it is possible to obtain the exact solution. For a single-component Fermi liquid, the general theory was developed in Refs. [36–38] and was extended to the multicomponent case in Refs. [6, 23]. In these references, the exact solution was given in analytical way in form of the rapidly converging series. Equivalently, the system of transport equations can be solved numerically.

Let me briefly outline the method of the exact solution of transport equations for the thermal conductivity and shear viscosity problems. Here I mainly follow the notations in Ref. [39]. Instead of Eq. (1), transport coefficients are rewritten in the form

$$\kappa_c = C_c^\kappa \frac{\pi^2 T n_c}{3m_c^*} \tau_{c0}, \quad \eta_c = C_c^\eta \frac{p_{Fc}^2 n_c}{5m_c^*} \tau_{c0}, \quad (41)$$

where the characteristic relaxation time

$$\tau_{c0}^{-1} = \nu_{c0} = \frac{3T^2 m_c^*}{8\pi^4 p_{Fc}} \sum_i m_i^{*2} \langle \mathcal{Q}_{ci} \rangle_{q\phi} \quad (42)$$

is introduced. By $\langle \cdot \rangle_{q\phi}$ in Eq. (42), the w -independent part of Eq. (7) is denoted. Characteristic relaxation times

are now the same for the thermal conductivity and for the shear viscosity. The differences between the specific transport problems are encapsulated in the coefficients C_c^κ and C_c^η . In order to find these coefficients, one starts from the system of transport equations for the non-equilibrium distribution functions $F_c(\mathbf{p}_c)$ for the particle species c . These equations are then linearized by introducing a correction to the local equilibrium distribution function as

$$F_c(\mathbf{p}_c) = f(x_c) + \tau_{c0} \Psi_c(x_c) D(\mathbf{p}_c) \frac{1}{T} \frac{\partial f(x_c)}{\partial x_c}, \quad (43)$$

where $f(x) = [1 + \exp(x)]^{-1}$ is the Fermi-Dirac distribution, $x_c = (\epsilon_c - \mu_c)/T$, μ_c is the chemical potential and $D(\mathbf{p})$ is the anisotropic part of the driving term. For the thermal conductivity, $D(\mathbf{p}) = \mathbf{v} \nabla T$ where \mathbf{v} is the particle velocity, while for the shear viscosity, $D(\mathbf{p}) = (v_\alpha p_\beta - 3^{-1} v p \delta_{\alpha\beta}) (\partial_\beta V_\alpha + \partial_\alpha V_\beta) / 2$, where \mathbf{V} is the hydrodynamical velocity with $\text{div} \mathbf{V} = 0$. Transport coefficients can be found by substituting Eq. (43) into the equations for the corresponding thermodynamic fluxes [22, 40]. This results in

$$C_c^\kappa = \frac{3}{\pi^2} \int_{-\infty}^{+\infty} dx x \Psi_c^\kappa(x) f(x) (1 - f(x)) \quad (44)$$

and

$$C_c^\eta = \int_{-\infty}^{+\infty} dx \Psi_c^\eta(x) f(x) (1 - f(x)). \quad (45)$$

Unknown functions $\Psi_c(x)$ obey the system of integral equations, derived by the linearization of the system of transport equations using ansatz (43). Without going into details [22, 23, 39], the resulting system of integral equations takes a form

$$\Xi(x) f(-x) = \left(1 + \frac{x^2}{\pi^2}\right) \Psi_c(x) f(-x) - \frac{2}{\pi^2} \int_{-\infty}^{+\infty} dx' f(-x') \frac{x - x'}{1 - e^{x' - x}} \sum_i \lambda_{ci} \Psi_i(x'), \quad (46)$$

where $\Xi(x) = 1$ for the shear viscosity and $\Xi(x) = x$ for the thermal conductivity. This simple form is possible due the appropriate choice of the relaxation time τ_{c0} by Eq. (42). All information about the quasiparticle scattering is encapsulated in the matrix λ_{ci} which depends on the transport coefficient in question. In case of thermal conductivity, this matrix can be expressed through the collision frequencies discussed in the previous sections in the following way:

$$\lambda_{ci}^\kappa = -\frac{5}{4} \frac{\nu_{ci}^{\kappa}}{\nu_{i0}}, \quad i \neq c, \quad (47)$$

$$\lambda_{cc}^\kappa = 3 - \frac{5}{4} \sum_i \frac{\nu_{ci}^\kappa}{\nu_{c0}} - \frac{5}{4} \frac{\nu_{cc}^{\kappa}}{\nu_{c0}}. \quad (48)$$

Simplest variational solution discussed above is $\Psi_c^\kappa = C_c^\kappa x_c$ and corresponds to the solution of the linear system $5/4 = \sum_i (3\delta_{ci} - \lambda_{ci}^\kappa) C_i^\kappa$. Once λ_{ci}^κ is calculated, the system (46) can be solved numerically and the correction coefficients C_c^κ can be obtained. It turns out, however, that $\lambda_{ci}^\kappa \approx \delta_{ci}$ in the conditions of the present study. This is because both ν_{ci}^κ and ν_{c0} are dominated by the transverse contribution in its leading order, while

the mixed collision frequencies ν'_{ci} are of the next order and thus their ratios to ν_{c0} are small. As a result, the system of equations (46) decouples to independent equations for each species. Therefore the correction to variational solution is given by the expression for the single-component Fermi liquid with $\lambda^\kappa = 1$. In this case, one obtains $C_c^\kappa/C_c^{\kappa, \text{Var}} = 1.2$, see, e.g., Ref. [22]. Numerical solution of Eq. (46) supports this conclusion, giving $\kappa_{e\mu}/\kappa_{e\mu}^{\text{Var}} \approx 1.20 - 1.22$ in all considered cases.

The situation is similar for the shear viscosity. The matrix λ_{ci}^η is

$$\lambda_{ci}^\eta = -\frac{3}{4} \frac{\nu'_{ci}{}^\eta}{\nu_{i0}}, \quad i \neq c, \quad (49)$$

$$\lambda_{cc}^\eta = 1 - \frac{3}{4} \sum_i \frac{\nu_{ci}^\eta}{\nu_{c0}} - \frac{3}{4} \frac{\nu'_{cc}{}^\eta}{\nu_{c0}}, \quad (50)$$

and simplest variational result is $\Psi_c^\eta = C_c^\eta$ and corresponds to the solution of the linear system $1 = \sum_i (\delta_{ci} - \lambda_{ci}^\eta) C_i^\eta$. In this case, since the collision frequencies for shear viscosity are q^2 in the leading order, in the weak-screening approximation they are much smaller than ν_{c0} . As a consequence, $\lambda_{ci}^\eta \approx \delta_{ci}$ as well. Moreover, this means that variational result does not need to be corrected and $\eta_{e\mu} = \eta_{e\mu}^{\text{Var}}$ [22]. Numerical calculations show that this conclusion holds up to 0.1% for the present conditions.

IV. DISCUSSION

The results of the previous sections can be used for calculating the lepton contribution to transport coefficients of superconducting NS cores at not-too-high temperatures. Since these coefficients are governed by the electromagnetic interactions, the obtained results are applicable for any $n\mu$ EOS of a neutron star core, provided the particle fractions and proton effective masses are known. It is clear from examining Eqs. (27)–(30), that the increase in proton fraction at a given baryon density lead to increase in both $\kappa_{e\mu}$ and $\eta_{e\mu}$. At the same time, the parameter A increases with x_p as well, so the crossover between the London and Pippard regimes occurs at lower n_B for the EOS with higher proton fraction. Specifically, results are illustrated for two EOSs, HHJ and BSk21, and as before, the proton effective mass $m_p^* = 0.8m_u$ is used. (The effect of effective mass variation is discussed separately below.) For completeness, all results discussed in this section employ exact solution of the system of transport equations taking into account all kinematical corrections as discussed in Secs. III C–III D.

Figure 7 shows the total lepton thermal conductivity $\kappa_{e\mu}$ as a function of n_B for the HHJ EOS [panel (a)] and the BSk21 EOS [panel (b)], $T = 10^8$ K and three values of $T_{cp} = 10^{10}$ K, 3×10^9 K, and 10^9 K. Remember, that the lepton thermal conductivity in a superconducting NS core scales as $\kappa_{e\mu} \propto T^{-1}$ as in the normal Fermi liquid. Solid lines give the results of the present

paper with the corrected description of the transverse screening. Dash-dotted lines are calculated taking the screening in the Pippard limit, as in Ref. [7]. According to Eq. (29), in this limit $\kappa_{e\mu}$ is approximately proportional to Δ . Clearly, these results strongly overestimate $\kappa_{e\mu}$, especially at lower densities and higher values of T_{cp} , which correspond to low values of the A parameter. The dashed lines in Fig. 7 show $\kappa_{e\mu}$ calculated employing the transverse screening in the London limit. In this limit, $\kappa_{e\mu}$ is independent of Δ , see Eq. (29), so only the single dashed line is present in Fig. 7. Thermal conductivity calculated in this limit also overestimates $\kappa_{e\mu}$. For low densities and/or high T_{cp} , this overestimation is small. For instance, for $T_{cp} = 10^{10}$ K, dashed lines give rather good approximation for $\kappa_{e\mu}$ (compare with the solid lines) for all shown densities and for both EOSs. In contrast, for high densities and $T_{cp} = 10^9$ K, the Pippard limit gives much better approximation than the London one. Comparing left and right panels of Fig. 7, one can see that the difference between $\kappa_{e\mu}$ calculated in the Pippard limit and the correct value is smaller for the BSk21 EOS than for the HHJ EOS. Similarly, the difference between the London-limit calculations and exact ones (solid lines) is larger for the BSk21 EOS than for the HHJ EOS. This is a consequence of the larger value of the A parameter for the BSk21 EOS (see Fig. 3). For comparison, with dotted lines in Fig. 7, $\kappa_{e\mu}^N$ calculated for the non-superconducting case is plotted. Again, all terms in the interaction are included, although the leading-order Eq. (15) gives a good approximation (notice, that correction to the variational solution is negligible in this case [7]). Since $\kappa_{e\mu}^N$ in leading order does not depend on temperature (see Sec. II), the difference between $\kappa_{e\mu}$ and $\kappa_{e\mu}^N$ increases with lowering T [7]. Taking this in mind and looking at the lower-density region in the left panel of Fig. 7 one can naively suggest that with increase of temperature, the normal-matter $\kappa_{e\mu}^N$ would become larger than $\kappa_{e\mu}$ for superconducting matter. This is not so, since in these conditions the assumption of the dominance of the proton contribution to the transverse screening will break down. In this case, one needs to include the dynamical contribution from the normal constituents of matter (leptons) to the transverse screening, see below. Presence of the normal matter contribution to screening effectively limits the collision frequencies from above, making them lower than in the normal case.

Similar calculations for the shear viscosity $\eta_{e\mu}$ are shown in Fig. 8. Qualitatively, the situation is the same as for the thermal conductivity, although the differences between results in various approximations are less dramatic. This is a consequence of, first, the weaker dependence of the transverse collision frequencies ν'_{ci} on the screening than found for ν_{ci}^κ and, second, of the larger contribution of the longitudinal part of the interaction to $\eta_{e\mu}$ than to $\kappa_{e\mu}$. For instance, the older results of Ref. [8] calculated in the Pippard limit (dash-dotted lines in Fig. 8) are acceptable for $T_{cp} < 3 \times 10^9$ K, especially at higher densities. At most, the use of the Pippard limit

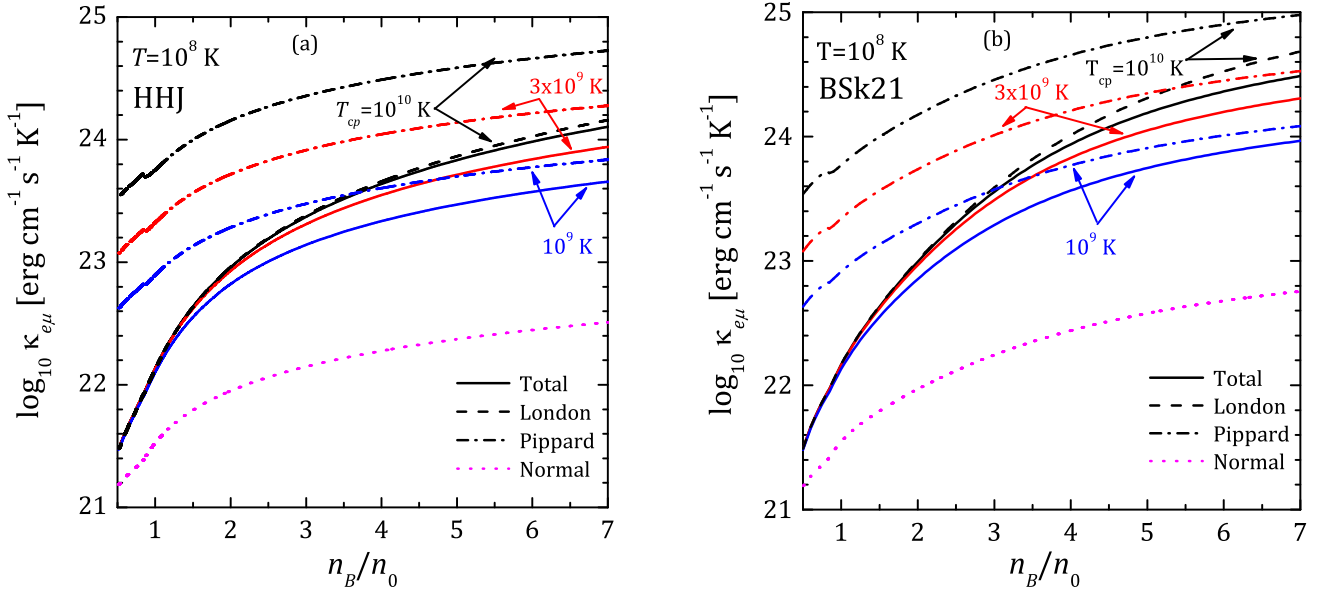


Figure 7. (Color online). Lepton thermal conductivity $\kappa_{e\mu}$ as a function of n_B (a) for the HHJ EOS and (b) for the BSK21 EOS, $T = 10^8$ K, and for three values of $T_{cp} = 10^{10}$, 3×10^9 , and 10^9 K as indicated in the plot. Solid lines show the results of the present paper, dash-dotted lines correspond to the Pippard limit, and dashed lines to the London limit of transverse screening. Dotted lines show the calculations for normal (not superconducting) matter.

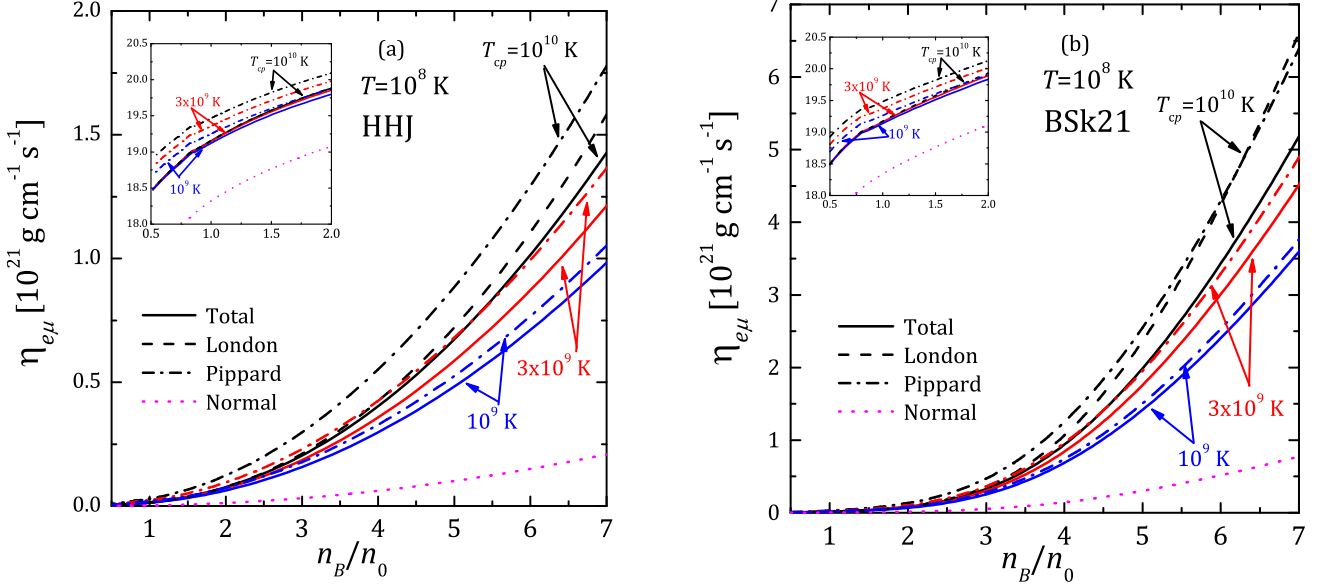


Figure 8. (Color online). Lepton shear viscosity (a) for the HHJ EOS and (b) for the BSK21 EOS as a function of n_B . The parameters of calculations and notations are the same as in Fig. 7. Notice, that the linear scale is used in this plot. Insets enlarge the region of n_B up to $2n_0$, where the logarithmic scale for $\eta_{e\mu}$ is used.

results in an overestimation of $\eta_{e\mu}$ by a factor of 2.5 for $T = 10^9$ K and lowest densities. This is not seen in Fig. 8 because of the linear scale, and is illustrated in the insets that show $\eta_{e\mu}$ up to $n_B = 2n_0$ with the logarithmic scale. In the inset plots, due to a low density, the difference between $\eta_{e\mu}$ calculated for various T_{cp} and those calculated in London limit is barely seen. On the other hand, the overestimation that results from using the Pip-

pard expression becomes visible. $\eta_{e\mu}^N$ calculated for non-superconducting matter is shown in Fig. 8 with dotted lines. Notice again, that the relation $\eta_{e\mu}^N \propto T^{-5/3}$ given by Eq. (16) works well only at low temperatures, where the transverse part of the interaction starts to dominate [8]. Both the shear viscosity and the thermal conductivity for the BSK21 EOS are larger than those for the HHJ EOS. This is a consequence of different particle number

fractions in these models.

In the previous discussion the constant (density-independent) proton effective mass was employed. It is instructive to look how the results depend on m_p^* . This is illustrated in Fig. 9 where the thermal conductivity [panel (a)] and shear viscosity [panel (b)] are plotted as a function of m_p^* for the density $n_B = 4n_0$ and proton fraction $x_p = 0.15$. These are some typical values and do not correspond to a specific EOS. The line types and notations are similar to those in Figs. 7-8. Asymptotic expression in the Pippard limit in the leading order, Eqs. (29)–(30) do not depend on the proton effective mass. Some dependence on m_p^* demonstrated by the dash-dotted lines in Fig. 9 is due to the corrections beyond the leading order. This dependence is more pronounced for the shear viscosity than for the thermal conductivity, in accordance with the discussion in Sec. III C. Similar arguments apply for the transport coefficients of the normal matter shown with dotted lines in Fig. 9. In contrast, the asymptotic expressions in the London limit, Eqs. (27)–(28) explicitly depend on the proton effective mass through the Meissner momentum q_M . According to Eq. (19), an increase in m_p^* leads to decrease in q_M and hence to decrease of $\kappa_{e\mu}$ and $\eta_{e\mu}$. As seen in Fig. 9, this decrease is larger for $\kappa_{e\mu}$ than for $\eta_{e\mu}$ because of the weaker q_M -dependence of the latter, see Eqs. (27)–(28). The dependence of the results of the full calculations on the effective mass is in between the discussed limiting cases. Since the parameter A decreases with m_p^* [see Eq. (21)], London limiting expressions work better for larger m_p^* . Figure 9 shows that the use of the variable proton effective mass instead of the constant m_p^* approximation can change the results illustrated in Figs. 7-8 quantitatively, but not qualitatively. In principle one should use the density dependence of m_p^* consistent with the chosen EOS, but this is rarely provided.

The proton critical temperature in the NS core is not constant but is actually density-dependent. It is instructive to illustrate the results by considering ‘realistic’ profiles $T_{cp}(n_B)$ in the NS core. This is done in Figs. 10 and 11 for the HHJ and the BSK21 EOSs, respectively.³ There exists a variety of calculations of the critical density profiles in a literature, each of which is based on a specific microscopic model. The results of these calculations generally do not agree with each other. In these circumstances it is instructive to rely on the phenomenological profiles $T_{cp}(n_B)$ instead of trying to handle EOS and superconductivity properties self-consistently [41, 42]. It is, however, reasonable to make these phenomenological models to resemble the extreme cases available on the market. Taking this in mind, following Glampedakis et al. [43], I take two profiles of $T_{cp}(n_B)$ denoted by ‘e’ and ‘f’ in Ref. [42]. These models are constructed by applying the phenomenological parametrization sug-

gested by Kaminker et al. [41] to the results of microscopic calculations of the proton 1S_0 gaps [42]. The critical temperature profiles for these models are shown in Fig. 10 for the HHJ EOS and in Fig. 11 for the BSK21 EOS with right vertical scales. The model ‘f’ describes weaker proton superconductivity based on the calculations in Ref. [44]. The corresponding panels in Figs. 10 and 11 are marked ‘weak SC’. Panels (b) and (d) in the same Figs., marked ‘strong SC’, show results for stronger proton superconductivity model ‘e’ that is fitted to the results of Ref. [45], see Ref. [42] for details. With the same right vertical scale in each panel the corresponding density-dependence of the parameter A is shown. Vertical dashed lines divide the regions of the superconductivity of the first and second types, according to the criterion $A > \sqrt{2}\pi$ ($\varkappa < 1/\sqrt{2}$). Notice that the critical temperature profiles for the same superconductivity models are different for different EOSs because they actually depend on the proton Fermi momentum p_{Fp} which differs in the HHJ and BSK21 EOSs at the same n_B .

The results for the shear viscosity $\eta_{e\mu}$ for the models ‘f’ and ‘e’ are shown in the panes (a) and (b), respectively, in Figs. 10 and 11. The thermal conductivity calculations are shown in panels (c) and (d) of the same figures. All calculations employ now $T = 10^7$ K in order to meet the zero-temperature approximation in a whole density region shown (the low-temperature approximation can break down near the walls of the critical density profile, where T_{cp} is low). All the values can be scaled by T^2 for shear viscosity (by T for thermal conductivity) provided the condition $T < 0.35T_{cp}$ is fulfilled in the density region of interest. As in Figs. 7–8, solid lines in Figs. 10–11 show the results of the full calculations, while dashed and dot-dashed lines are calculated in the London and Pippard limits, respectively. Dotted lines represent the lepton transport coefficients in normal matter. The results in Figs. 10–11 follow the same pattern as discussed above. The use of any of the limiting expressions, London or Pippard, for the transverse screening leads to an overestimation of the transport coefficients. The London limit is appropriate in the case of type-II superconductivity, while in the case of type-I superconductivity, the London limit is inappropriate and the Pippard limit can be a better approximation. In the intermediate case full calculations should be used. As seen from Figs. 10–11, in the real situation, both types of superconductivity can be simultaneously present in the NS cores [43].

For comparison, in Figs. 10–11 I also show the neutron shear viscosity η_n and thermal conductivity κ_n calculated following Refs. [12, 39]. In these Refs., the in-medium nucleon-nucleon interaction is treated in the Brueckner-Hartree-Fock framework with the inclusion of the effective three-body forces. The hatched strips in Figs. 10–11 show the results for normal (non-superconducting) beta-equilibrated matter, and the widths of the strips illustrate the uncertainty in calculations related to the different models of the nuclear interactions as considered in Ref. [39]. The lower boundaries correspond to the nu-

³ Note that again $m_p^* = 0.8m_u$.

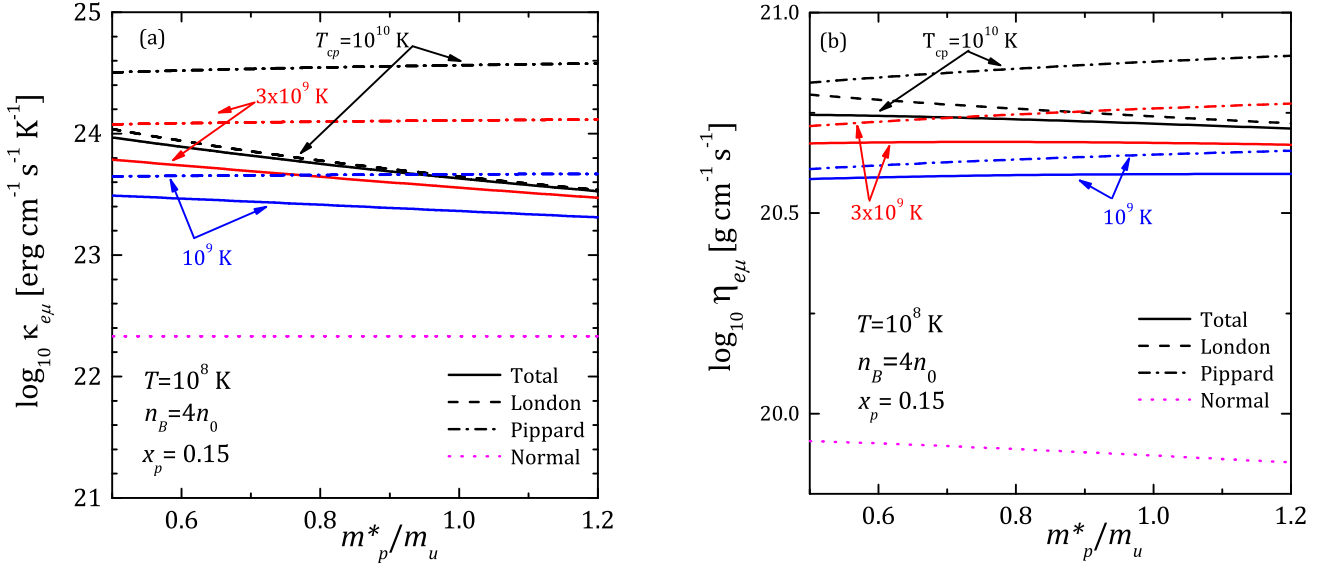


Figure 9. (Color online). Lepton thermal conductivity (a) and shear viscosity (b) calculated for $T = 10^8$ K, $n_B = 4n_0$, and proton fraction $x_p = 0.15$ as functions of the proton effective mass m_p^* . The notations are the same as in Fig. 7.

clear interaction described by the Argonne v18 potential with addition of the three-body forces in the phenomenological Urbana IX model. Upper boundaries correspond to the same potential, but another model for the three-body interaction based on the meson-nucleon model of the nucleon interactions. More details can be found in Refs. [39, 46]. Filled strips in Figs. 10–11 represent calculations of κ_n and η_n for the proton-superconducting matter. As in the case of the lepton transport coefficients, these results are obtained by neglecting the collisions with protons (they are damped exponentially in the considered limit). Then the neutron contribution to transport coefficients is mediated by the neutron-neutron collisions only. Notice, that the results for the neutron transport coefficients shown in Figs. 10–11 include the corrections to variational solution [12, 39]. Since κ_n and η_n are calculated within specific models of the nucleon interaction, the obtained results are not self-consistent with EOSs used elsewhere in the present paper. However, one expects that the results shown here give plausible estimates for the nucleon contribution (see Refs. [12] and [4] for more discussion).

Since neutron-proton collisions are damped in the superconducting matter, respective κ_n and η_n values are larger than those in normal matter (see, e.g. [8, 47]). However this increase is much smaller than the increase in lepton transport coefficients, which are additionally boosted by the change of the screening behavior. According to Figs. 10–11, the relation between lepton and neutron transport coefficients remains qualitatively the same as in the non-superfluid matter. Namely, $\kappa_n > \kappa_{e\mu}$, while $\eta_n < \eta_{e\mu}$. Remember (Sec. II) that the neutron transport coefficients obey the standard Fermi-liquid behavior $\kappa_n \propto T^{-1}$, $\eta_n \propto T^{-2}$ as do the lepton transport coefficients in proton-superconducting matter.

All calculations above rely on the zero-temperature approximation $T/\Delta \lesssim 0.2$. In this limit, it is enough to use the expressions (18)–(20) for the proton part of the transverse screening. Since this screening is static, the lepton dynamical screening, which in the leading order is proportional to ω , see Eq. (14), was neglected. In the Pippard limit this is possible when $\omega \ll \pi\Delta/r$, where $r = (p_{Fe}^2 + p_{F\mu}^2)/p_{Fp}^2 \approx 1$. Since typically $\omega \sim T$, this is always justified in our approximation. In the London limit, the similar comparison requires $\omega \sim T \ll 4/(3\pi)q_M v_{Fp}/r$. This requirement becomes stronger with lowering density, and transforms to $T \ll 10^9$ K for the BSk21 and HHJ EOSs at $n_B \approx 0.5n_0$.

When temperature starts to increase, the superfluid density of protons n_{sp} decreases and the Meissner momentum $q_M \propto n_{sp}^{1/2}$ also decreases. The screening becomes temperature-dependent. However, at low q it is approximately constant, moreover the change of the screening behavior from the London one to the Pippard one occurs at the temperature-independent value $q \sim \xi_0^{-1}$, where $\xi_0 \equiv \xi(T=0)$ [28]. Therefore, qualitatively, the results of the above analysis hold if one takes $A = \pi q_M(T)\xi_0$ (now A is not related to \varkappa which is independent of T). At a given density, A decreases with increase of temperature making London limiting expressions more appropriate. Transport coefficients start to decrease, and in the leading order their temperature behavior is given by Eqs. (27)–(28), providing temperature-dependent $q_M(T)$ is used in this case. Such approach is possible until the dynamical part of the proton polarization function and the lepton contribution (14) start to be important. Thus, at the intermediate temperature the ω dependence of the transverse polarization function needs to be taken into account, that complicates the calculations [7, 8]. In the same region, the lepton-proton colli-

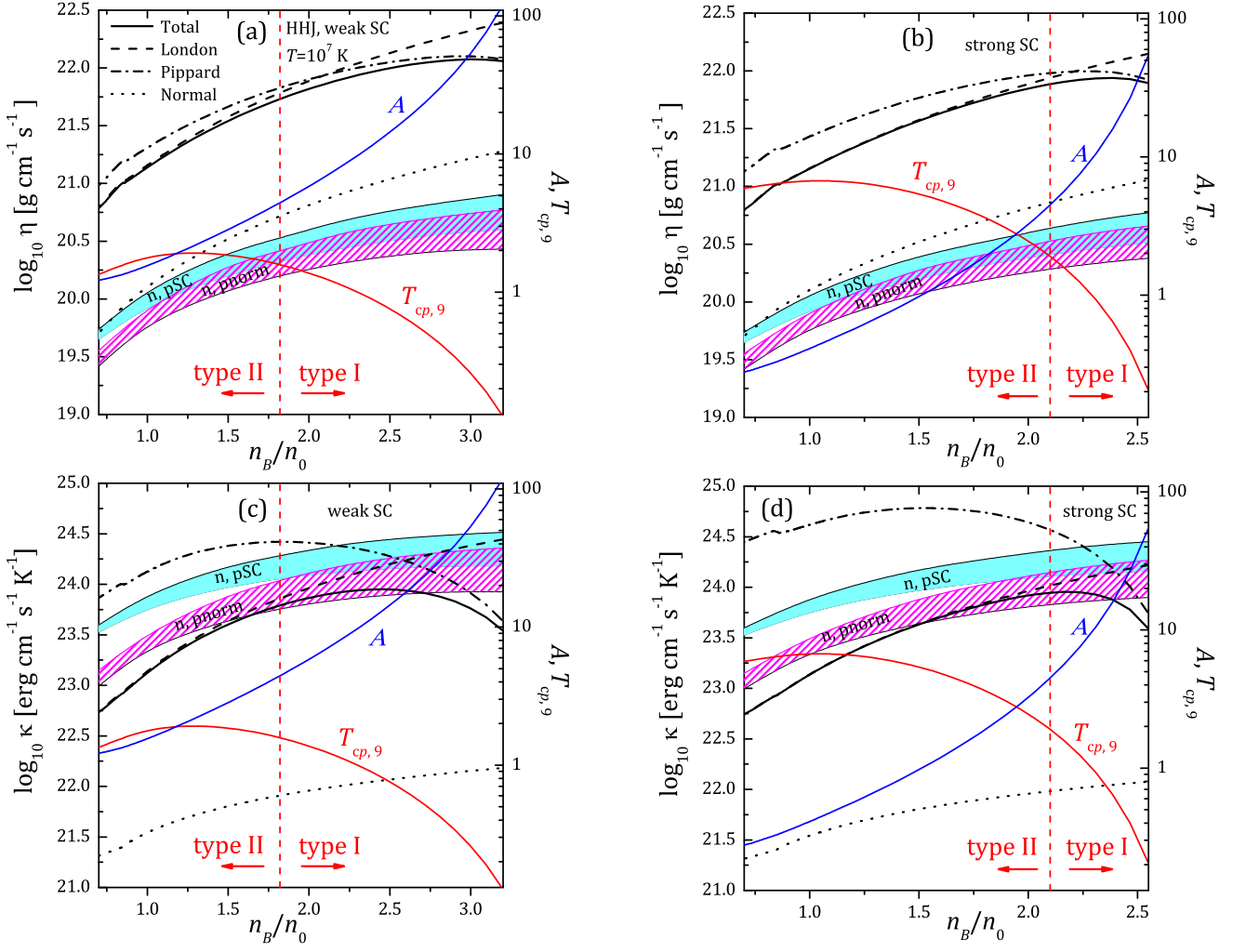


Figure 10. (Color online). Shear viscosity (a)–(b) and thermal conductivity (c)–(d) in the HHJ NS core for weak proton superconductivity model [panels (a) and (c)] and strong superconductivity model [panels (b) and (d)] discussed in the text. Temperature is set to $T = 10^7$ K. As in previous figures, solid lines give full results of the present work, dash-dotted lines correspond to calculations in the Pippard limit, and dashed lines – to calculations in London limit. Dotted lines show the transports coefficients in normal matter. Lower hatched strips marked ‘n, pnorm’ and upper filled strips marked ‘n, pSC’ give the uncertainty bands for neutron transport coefficients in normal and superconducting matter, respectively. Thin solid lines and the right scales in each panel show the values of $T_{cp,9} = T_{cp}/10^9$ K and A for each model. Vertical dashed lines ($A = \sqrt{2}\pi$) divide type-II and type-I superconductivity regions. See text for details

sions start to be important that additionally decrease the transport coefficients. The consideration of the lepton-proton collisions is less straightforward since in the region of small momenta $qv_{Fp} \sim \Delta$ the renormalization of the proton current is necessary (e.g., [27, 48]). In addition, because of the gap in the proton spectrum, typical transferred energy is of the order of Δ and the limiting approximation $qv_{Fp} \gg \omega$ is not justified in the London limit. Fortunately, due to the exponential suppression of the lepton-proton collision frequencies, these effects need to be taken into account relatively close to the critical temperature where $\Delta(T) \sim T$. Then the approximation $qv_{Fp} \gg \omega$ is valid since $\omega \sim \Delta \sim T$. Clearly, the calculations of the transport coefficients in the transition region $0.35T_{cp} \lesssim T \lesssim T_{cp}$ are more involved than in the sim-

ple zero-temperature case. However, it seems sufficient in applications to construct the smooth interpolation between the results of the present paper at $T < 0.35T_{cp}$ and the normal matter results at $T > T_{cp}$.

V. CONCLUSIONS

I have calculated the electron and muon shear viscosity $\eta_{e\mu}$ and thermal conductivity $\kappa_{e\mu}$ in the proton-superconducting core of the NS based on the transport theory of the Fermi systems. The present results are applicable at the low temperatures, $T \lesssim 0.35T_{cp}$, and differ from available calculations [7, 8] by the corrected account of the screening of the electromagnetic interaction when

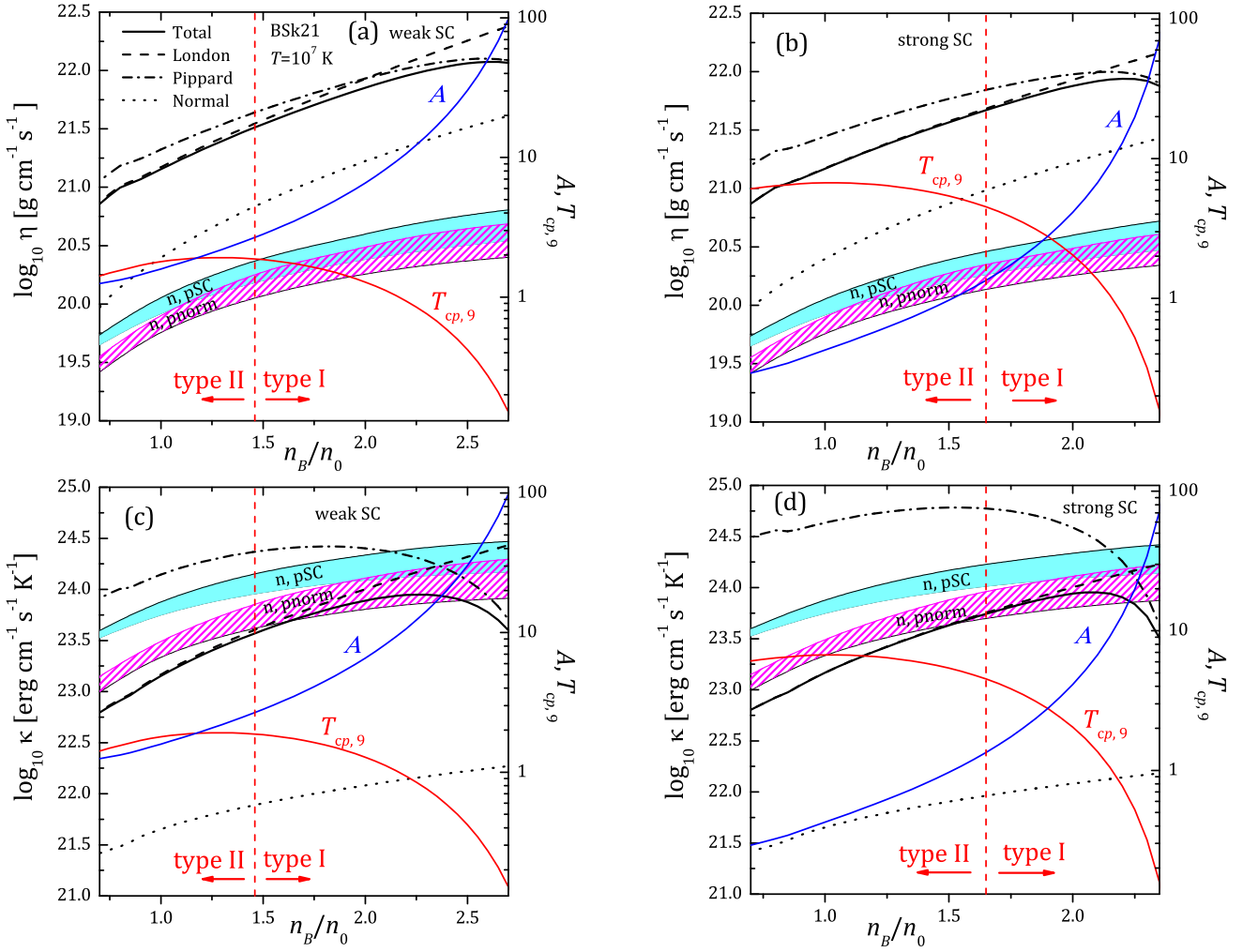


Figure 11. (Color online). Same as Fig. 10 but for the BSk21 EOS. Notations are the same as in Fig. 10.

the protons are in the paired state.

The variational results for the thermal conductivity and for the shear viscosity are obtained from Eqs. (1)–(2) using the appropriate collision frequencies. According to Secs. III B–III C, Eq. (23) with Eq. (A.3) can be used for thermal conductivity calculations. For the shear viscosity, it is enough to use the leading-order contributions in q in Eqs. (35)–(38). The explicit expressions for these contributions are given by Eqs. (A.5)–(A.7). Finally, the simplest variational solution works well for $\eta_{e\mu}$, while for $\kappa_{e\mu}$ additional factor $C^\kappa = 1.2$ should be used in Eq. (1) to correct the variational result.

The main conclusions of the present study are as follows:

- (i) In the superconducting NS cores, lepton transport coefficients obey the standard Fermi-liquid temperature dependence $\kappa_{e\mu} \propto T^{-1}$, $\eta_{e\mu} \propto T^{-2}$ in contrast to the situation in normal NS cores where $\kappa_{e\mu} \approx \text{const}(T)$, $\eta_{e\mu} \propto T^{-5/3}$. This is a consequence of the static regime of the screening of electromagnetic interactions. The screening in the

transverse channel is dominated by the proton contribution.

- (ii) At a given density, $\kappa_{e\mu}$ and $\eta_{e\mu}$ increase with increase of the proton critical temperature T_{cp} (increase of the gap Δ). At large densities, where the typical transferred momentum q is large so that the Pippard limit for the transverse screening is applicable, one finds $\kappa_{e\mu} \propto \Delta$ and $\eta_{e\mu} \propto \Delta^{1/3}$. In the opposite limit of low densities, where the transverse electromagnetic interaction is screened by the Meissner momentum (the London limit), $\kappa_{e\mu}$ and $\eta_{e\mu}$ are independent of Δ .
- (iii) In general situation relevant for the NS cores, the whole range of momentum transfer is important, both limiting expressions overestimate transport coefficients, and the complete results developed here shall be used. However, in case of the superconductivity of the second kind it is enough to take the London limit for transverse screening and use corresponding limiting expressions for the trans-

verse part of the collision frequencies. In case of the type-I superconductivity, the Pippard limit is more appropriate, although it is recommended to rely on the complete result in this limit.

- (iv) Both limiting expressions can be used to estimate the transport coefficients from above. In this respect, the expression in London limit is more interesting since it gives the gap-independent boundary.
- (v) As in the case of the normal matter [4, 12], leptons give dominant contribution to the shear viscosity while neutrons dominate the thermal conductivity.

Since the consideration of the lepton transport coefficients presented here does not rely of the specific EOS properties, the conclusions (i)–(iv) are universal in a sense that they are valid for any $npe\mu$ EOS of the dense matter in NS cores. In contrast, the conclusion (v) is model-dependent and need to be taken with caution. The neutron transport coefficients shown in Figs. 10–11 are calculated for different nucleon interactions, but within the single many-body approach, namely the Brueckner-Hartree-Fock scheme. Thus it is in principle not excluded that the conclusion (v) can fail for a specific microscopic model that produces significantly different values of κ_n and η_n than used here. Ideally, the neutron transport coefficients need to be calculated from the same microscopic model of the nucleon interaction as the EOS which is not a straightforward task. The detailed discussion of the neutron transport coefficients is outside the scope of the present paper, see Refs. [4, 12] for more details.

The results obtained in the present paper can be improved by considering the finite temperature effects in order to study in detail the transition from the superconducting to the normal matter. This can be done following the same lines as described here, but considering the full temperature-dependent polarization functions. In this case, however, one needs to account for the dynamical part of the screening making the interaction ω -dependent. In this case the integration over ω

in Eqs. (3)–(6) cannot be performed analytically. Additional care must be taken when lepton collisions with the protonic excitations are considered. Anyway, it seems enough to interpolate through the transition region for practical applications, however the detailed investigation of the transition region remains to future studies.

In this paper I used polarization functions calculated in pure BCS framework, neglecting Fermi-liquid effects. In the Pippard limit this is a good approximation [26]. However, the static screening in the London limit is affected [26]. The consideration of these effects requires separate study. Moreover, it was proposed that the coupling between neutrons and protons in NS cores induces the effective electron-neutron interaction [49] that modifies the screening properties of matter [50] and can affect the lepton collision frequencies. The effect of this interaction on the transport coefficients can be expected both in the normal and superconducting matter and is under investigation [50].

In the inner cores of NSs, hyperons can also appear [1]. If they are normal (unpaired), the results of the present paper for lepton transport coefficients can be easily generalized by treating charged hyperons as passive scatterers. It is thought, however, that hyperons like the protons can be paired in the 1S_0 channel (since their number density is low), see e.g. review in Ref. [19]. In this case, their contribution to the transverse plasma screening should be considered in the same way as the proton one, although the situation will be more cumbersome since more than one gap is involved.

ACKNOWLEDGMENTS

The author is grateful to N. Chamel, M. E. Gusakov, and D. G. Yakovlev for discussions. The work was supported by the Foundation for the Advancement of Theoretical Physics and Mathematics “BASIS” and the Russian Foundation for Basic Research, grant 16-32-00507 mol-a.

-
- [1] P. Haensel, A. Y. Potekhin, and D. G. Yakovlev, *Neutron Stars 1: Equation of State and Structure*, vol. 326 of *Astrophysics and Space Science Library* (Springer Science+Buisness Media, New York, 2007).
 - [2] V. M. Kaspi, Proceedings of the National Academy of Science **107**, 7147 (2010), 1005.0876.
 - [3] B. P. Abbott et al. (LIGO Scientific Collaboration and Virgo Collaboration), Phys. Rev. Lett. **119**, 161101 (2017).
 - [4] A. Schmitt and P. Shternin, ArXiv e-prints (2017), 1711.06520.
 - [5] A. Y. Potekhin, J. A. Pons, and D. Page, Space Sci. Rev. **191**, 239 (2015), 1507.06186.
 - [6] E. Flowers and N. Itoh, Astrophys. J. **230**, 847 (1979).
 - [7] P. S. Shternin and D. G. Yakovlev, Phys. Rev. D **75**, 103004 (2007), 0705.1963.
 - [8] P. S. Shternin and D. G. Yakovlev, Phys. Rev. D **78**, 063006 (2008), 0808.2018.
 - [9] P. S. Shternin, JETP **107**, 212 (2008).
 - [10] H. Heiselberg, G. Baym, C. J. Pethick, and J. Popp, Nucl. Phys. A **544**, 569 (1992).
 - [11] H. Heiselberg and C. J. Pethick, Phys. Rev. D **48**, 2916 (1993).
 - [12] P. S. Shternin, M. Baldo, and P. Haensel, Phys. Rev. C **88**, 065803 (2013), 1311.4278.
 - [13] E. E. Kolomeitsev and D. N. Voskresensky, Phys. Rev. C **91**, 025805 (2015), 1412.0314.
 - [14] O. Benhar and M. Valli, Phys. Rev. Lett. **99**, 232501 (2007), 0707.2681.

- [15] H. F. Zhang, U. Lombardo, and W. Zuo, *Phys. Rev. C* **82**, 015805 (2010), 1006.2656.
- [16] U. Lombardo and H.-J. Schulze, in *Physics of Neutron Star Interiors*, edited by D. Blaschke, N. K. Glendenning, and A. Sedrakian (2001), vol. 578 of *Lecture Notes in Physics, Berlin Springer Verlag*, p. 30, astro-ph/0012209.
- [17] D. Page, J. M. Lattimer, M. Prakash, and A. W. Steiner, in *Novel Superfluids: Volume 2*, edited by K. H. Bennemann and J. B. Ketterson (Oxford University Press, 2014), p. 505, 1302.6626.
- [18] B. Haskell and A. Sedrakian, *ArXiv e-prints* (2017), 1709.10340.
- [19] A. Sedrakian and J. W. Clark, *ArXiv e-prints* (2018), 1802.00017.
- [20] A. Gezerlis, C. J. Pethick, and A. Schwenk, *ArXiv e-prints* (2014), 1406.6109.
- [21] D. G. Yakovlev and C. J. Pethick, *Ann. Rev. Astron. Astrophys.* **42**, 169 (2004), astro-ph/0402143.
- [22] G. Baym and C. Pethick, *Landau Fermi-Liquid Theory: Concepts and Applications* (John Wiley & Sons, inc., New York, Chichester, Brisbane, Toronto, Singapore, 1991).
- [23] R. H. Anderson, C. J. Pethick, and K. F. Quader, *Phys. Rev. B* **35**, 1620 (1987).
- [24] M. G. Alford, H. Nishimura, and A. Sedrakian, *Phys. Rev. C* **90**, 055205 (2014), 1408.4999.
- [25] K. P. Levenfish and D. G. Yakovlev, *Astronomy Reports* **38**, 247 (1994).
- [26] M. E. Gusakov, *Phys. Rev. C* **81**, 025804 (2010), 1001.4452.
- [27] P. I. Arseev, S. O. Loiko, and N. K. Fedorov, *Physics Uspekhi* **49**, 1 (2006).
- [28] E. Lifshitz and L. Pitaevskii, *Statistical Physics. Part 2., Course of theoretical physics by L. D. Landau and E. M. Lifshitz, Vol. 9* (Butterworth-Heinemann, 1980).
- [29] H. Heiselberg and M. Hjorth-Jensen, *Astrophys. J. Lett.* **525**, L45 (1999), astro-ph/9904214.
- [30] A. Akmal, V. R. Pandharipande, and D. G. Ravenhall, *Phys. Rev. C* **58**, 1804 (1998), nucl-th/9804027.
- [31] M. E. Gusakov, A. D. Kaminker, D. G. Yakovlev, and O. Y. Gnedin, *Mon. Not. R. Astron. Soc.* **363**, 555 (2005), astro-ph/0507560.
- [32] A. Y. Potekhin, A. F. Fantina, N. Chamel, J. M. Pearson, and S. Goriely, *Astron. Astrophys.* **560**, A48 (2013), 1310.0049.
- [33] D. R. Tilley and J. Tilley, *Superfluidity and Superconductivity (Graduate Student Series in Physics)* (Institute of Physics Publishing, Bristol, UK, 1990), 1st ed.
- [34] A. Haber and A. Schmitt, *Phys. Rev. D* **95**, 116016 (2017), 1704.01575.
- [35] G. Baym, C. Pethick, and D. Pines, *Nature (London)* **224**, 673 (1969).
- [36] G. A. Brooker and J. Sykes, *Phys. Rev. Lett.* **21**, 279 (1968).
- [37] J. Sykes and G. A. Brooker, *Annals of Physics* **56**, 1 (1970).
- [38] H. Højgård Jensen, H. Smith, and J. W. Wilkins, *Phys. Lett. A* **27**, 532 (1968).
- [39] P. Shternin, M. Baldo, and H. Schulze, *Journal of Physics Conference Series* **932**, 012042 (2017).
- [40] L. Pitaevskii and E. Lifshitz, *Physical Kinetics, Course of theoretical physics by L. D. Landau and E. M. Lifshitz, Vol. 10* (Butterworth-Heinemann, 2008).
- [41] A. D. Kaminker, P. Haensel, and D. G. Yakovlev, *Astron. Astrophys.* **373**, L17 (2001), astro-ph/0105047.
- [42] N. Andersson, G. L. Comer, and K. Glampedakis, *Nuclear Physics A* **763**, 212 (2005), astro-ph/0411748.
- [43] K. Glampedakis, N. Andersson, and L. Samuelsson, *Mon. Not. R. Astron. Soc.* **410**, 805 (2011), 1001.4046.
- [44] L. Amundsen and E. Østgaard, *Nucl. Phys. A* **437**, 487 (1985).
- [45] Ø. Elgarøy, L. Engvik, M. Hjorth-Jensen, and E. Osnes, *Phys. Rev. Lett.* **77**, 1428 (1996), nucl-th/9604041.
- [46] M. Baldo, G. F. Burgio, H.-J. Schulze, and G. Taranto, *Phys. Rev. C* **89**, 048801 (2014).
- [47] D. A. Baiko, P. Haensel, and D. G. Yakovlev, *Astron. Astrophys.* **374**, 151 (2001), astro-ph/0105105.
- [48] J. Kundu and S. Reddy, *Phys. Rev. C* **70**, 055803 (2004), nucl-th/0405055.
- [49] B. Bertoni, S. Reddy, and E. Rrapaj, *Phys. Rev. C* **91**, 025806 (2015), 1409.7750.
- [50] S. Stetina, E. Rrapaj, and S. Reddy, *Phys. Rev. C* **97**, 045801 (2018), 1712.05447.

Appendix: Fitting expressions for integrals

The transverse integrals (22) can be normalized as

$$I_n = q_M^{3-n} \tilde{I}_n(x_t, A), \quad (\text{A.1})$$

where $x_t = q_M/q_m$ and

$$\tilde{I}_n(x_t, A) = \int_0^{1/x_t} \frac{x^n dx}{(x^2 + J(Ax))^2}. \quad (\text{A.2})$$

The integrals $\tilde{I}_n(x_t, A)$ were calculated on the dense grid and fitted by analytical expressions that take into account the correct asymptotic behavior in the limiting cases.

For $n = 0$ the result is

$$\frac{p_1 A^{1.5} + p_2 A^2 + \pi/4 - x_t^3/3 + p_3 x_t^4 + A(p_4 - p_5 x_t^3)}{1 + p_6 A}, \quad (\text{A.3})$$

where $p_1 = 0.0119$, $p_2 = 0.0063$, $p_3 = 0.202$, $p_4 = 0.108$, $p_5 = 0.454$, and $p_6 = 0.14$. Fit rms error is 0.4% and the maximal fitting error is 3% at $A = 5$ and $x_t = 0.76$.

Similarly, for $n = 2$.

$$(1 + p_6 A)^{-1} \left[p_1 A^{4/3} + \frac{\pi}{4} - x_t - p_2 A x_t + p_3 x_t^2 + A^{2/3} (p_4 + p_5 x_t) + A^{1/3} (p_7 - p_8 x_t + p_9 x_t^2) \right], \quad (\text{A.4})$$

where $p_1 = 0.094$, $p_2 = 0.234$, $p_3 = 0.356$, $p_4 = 0.1859$, $p_5 = 0.0496$, $p_6 = 0.227$, $p_7 = -0.0537$, $p_8 = -0.2345$, and $p_9 = 0.239$. Fit rms error is $\sim 1\%$ and the maximal fitting error is 7% at $A = 0.5$ and $x_t = 0.14$.

The leading-order contributions to the collision frequencies relevant for the shear viscosity problem (36)–(38) can be given as

$$\nu_{ci}^{\eta,t} = \frac{2\pi\alpha_f^2 T^2 p_{Fi}^2}{m_c^* p_{Fc}} I_2^t, \quad (\text{A.5})$$

$$\nu_{ci}^{\eta,l} = \frac{2\pi\alpha_f^2 T^2 m_c^* m_i^{*2}}{p_{Fc}^3 q_{TF}} \left(\arctan \frac{q_m}{q_{TF}} + \frac{q_{TF} q_m}{q_{TF}^2 + q_m^2} \right), \quad (\text{A.6})$$

$$\nu'_{ci}{}^\eta = \frac{4\pi\alpha_f^2 T^2 m_i^* p_{Fi}}{p_{Fc}^2 q_{TF}} \arctan \frac{q_m}{q_{TF}}. \quad (\text{A.7})$$